

# An esterase-responsive ibuprofen nano-micelle pre-modified embryo derived nucleus pulposus progenitor cells promote the regeneration of intervertebral disc degeneration

Kai-shun Xia<sup>a,b,c,d,1</sup>, Dong-dong Li<sup>e,1</sup>, Cheng-gui Wang<sup>f,1</sup>, Li-wei Ying<sup>g</sup>, Jing-kai Wang<sup>a,b,c,d</sup>, Biao Yang<sup>a,b,c,d</sup>, Jia-wei Shu<sup>a,b,c,d</sup>, Xian-peng Huang<sup>a,b,c,d</sup>, Yu-ang Zhang<sup>a,b,c,d</sup>, Chao Yu<sup>a,b,c,d</sup>, Xiao-peng Zhou<sup>a,b,c,d</sup>, Fang-cai Li<sup>a,b,c,d</sup>, Nigel K.H. Slater<sup>h</sup>, Jian-bin Tang<sup>e,\*\*\*</sup>, Qi-xin Chen<sup>a,b,c,d,\*\*</sup>, Cheng-zhen Liang<sup>a,b,c,d,\*</sup>

<sup>a</sup> Department of Orthopedics, 2nd Affiliated Hospital, School of Medicine, Zhejiang University, Hangzhou, 310009, Zhejiang, PR China

<sup>b</sup> Orthopedics Research Institute of Zhejiang University, Zhejiang University, Hangzhou, 310009, Zhejiang, PR China

<sup>c</sup> Key Laboratory of Motor System Disease Research and Precision Therapy of Zhejiang Province, Hangzhou, 310009, Zhejiang Province, PR China

<sup>d</sup> Clinical Research Center of Motor System Disease of Zhejiang Province, Hangzhou, 310009, Zhejiang Province, PR China

<sup>e</sup> Key Laboratory of Biomass Chemical Engineering of Ministry of Education Center for Bionanoengineering, Collage of Chemical and Biological Engineering, Zhejiang University, Hangzhou, 310027, Zhejiang, PR China

<sup>f</sup> The Second Affiliated Hospital and Yuying Children's Hospital of Wenzhou Medical University, Wenzhou, 325000, Zhejiang, PR China

<sup>g</sup> Orthopedic Department, Taizhou Hospital Affiliated to Wenzhou Medical University, Linhai, 317099, Zhejiang, PR China

<sup>h</sup> Department of Chemical Engineering and Biotechnology, University of Cambridge, Cambridge, United Kingdom

## ARTICLE INFO

### Keywords:

Intervertebral disc degeneration  
Nucleus pulposus progenitor cells  
Esterase-responsive nano micell  
Biomaterial pre-modification  
Synergistic transplantation therapy

## ABSTRACT

Stem cell-based transplantation is a promising therapeutic approach for intervertebral disc degeneration (IDD). Current limitations of stem cells include with their insufficient cell source, poor proliferation capacity, low nucleus pulposus (NP)-specific differentiation potential, and inability to avoid pyroptosis caused by the acidic IDD microenvironment after transplantation. To address these challenges, embryo-derived long-term expandable nucleus pulposus progenitor cells (NPPCs) and esterase-responsive ibuprofen nano-micelles (PEG-PIB) were prepared for synergistic transplantation. In this study, we propose a biomaterial pre-modification cell strategy; the PEG-PIB were endocytosed to pre-modify the NPPCs with adaptability in harsh IDD microenvironment through inhibiting pyroptosis. The results indicated that the PEG-PIB pre-modified NPPCs exhibited inhibition of pyroptosis *in vitro*; their further synergistic transplantation yielded effective functional recovery, histological regeneration, and inhibition of pyroptosis during IDD regeneration. Herein, we offer a novel biomaterial pre-modification cell strategy for synergistic transplantation with promising therapeutic effects in IDD regeneration.

## 1. Introduction

Current evidence suggests that approximately 70–90% of the global population are or will suffer from intervertebral disc degeneration (IDD) caused by low back pain once in their life [1,2]. The loss of the adult nucleus pulposus (NP) cells is considered one of the main factors of IDD,

which lead to the reduction of glycosaminoglycan and collagen II, and affect the function of human IVDs [3,4]. A promising strategy to improve the function of the damaged intervertebral disc (IVD) is to induce de novo regeneration of NP tissue through the integration of transplanted stem cells [5]. However, most studies have predominantly conducted transplantation of either mesenchymal stem cells (MSCs) [6] or

Peer review under responsibility of KeAi Communications Co., Ltd.

\* Corresponding author. Department of Orthopedics, 2nd Affiliated Hospital, School of Medicine, Zhejiang University, Hangzhou, 310009, Zhejiang, PR China.

\*\* Corresponding author. Department of Orthopedics, 2nd Affiliated Hospital, School of Medicine, Zhejiang University, Hangzhou, 310009, Zhejiang, PR China.

\*\*\* Corresponding author. Key Laboratory of Biomass Chemical Engineering of Ministry of Education Center for Bionanoengineering, Collage of Chemical and Biological Engineering, Zhejiang University, Hangzhou, 310027, Zhejiang, PR China.

E-mail addresses: [jianbin@zju.edu.cn](mailto:jianbin@zju.edu.cn) (J.-b. Tang), [zrcqx@zju.edu.cn](mailto:zrcqx@zju.edu.cn) (Q.-x. Chen), [liangchengzhen@zju.edu.cn](mailto:liangchengzhen@zju.edu.cn) (C.-z. Liang).

<sup>1</sup> These authors contributed equally to this work.

<https://doi.org/10.1016/j.bioactmat.2022.07.024>

Received 6 April 2022; Received in revised form 16 July 2022; Accepted 21 July 2022

2452-199X/© 2022 The Authors. Publishing services by Elsevier B.V. on behalf of KeAi Communications Co. Ltd. This is an open access article under the CC BY-NC-ND license (<http://creativecommons.org/licenses/by-nc-nd/4.0/>).

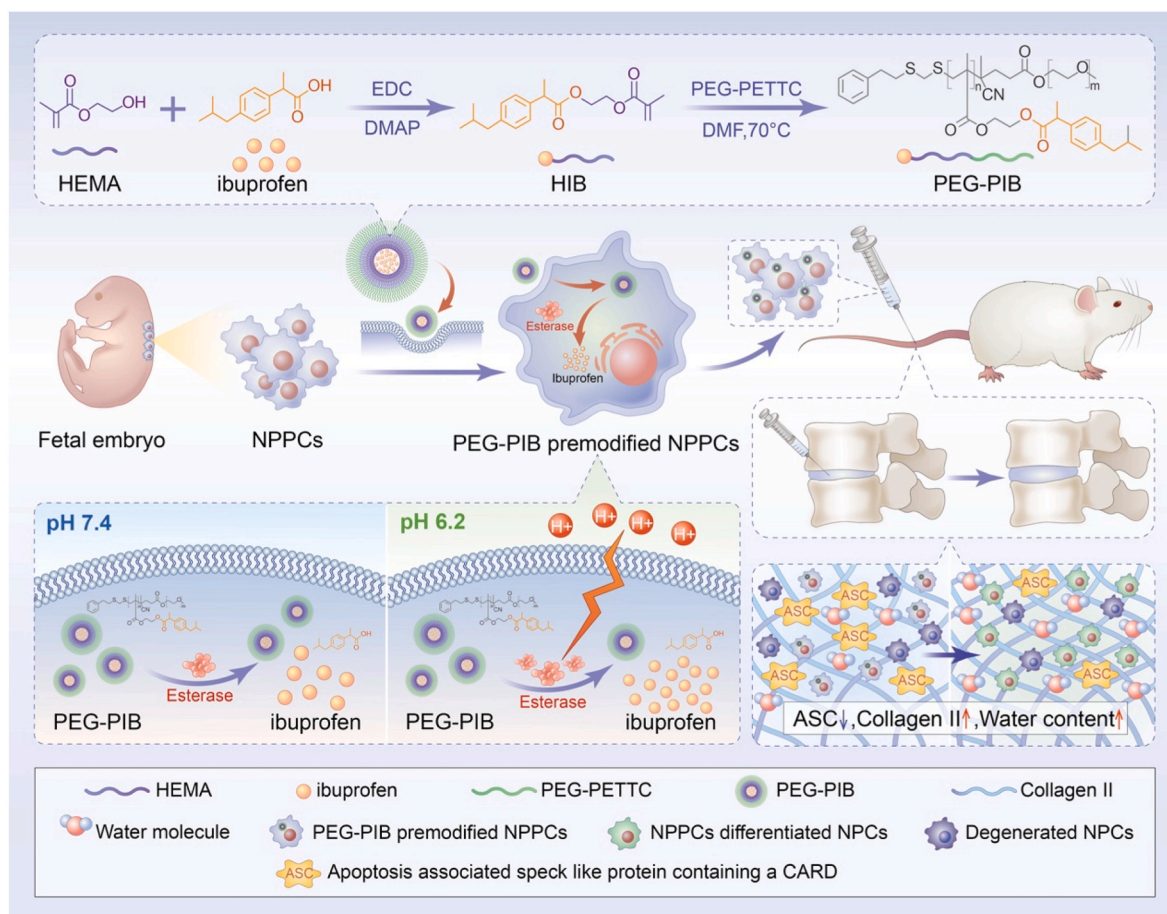
pluripotent stem cells (PSCs) [7], both of which exhibit unsatisfactory IDD regeneration performance in hypoxia, acidulous and inflammatory IDD microenvironment [8]. An increasing body of evidence suggests that despite their NP-specific differentiation potential and anti-inflammatory capacity, the intra-discal injection of “naked” MSCs is hampered by the harsh IDD microenvironment, resulting in poor survival rates, and altered activity [9–13]. PSCs are mainly restricted by the tumorigenesis risk, and their efficiency for NP-specific differentiation warrants more studies [14–23] (see Scheme 1).

Nucleus pulposus progenitor cells (NPPCs) originating from the NP tissue are reportedly the ideal cell source for IDD transplantation. NPPCs are considered an intermediate state of notochord cells gradually replaced by the NP cells (NPCs). Over the years, NPPCs from rats, pigs, humans and many other species [24–28] have been identified, possessing typical but fragmented vacuoles, similar stem cell characteristics, high efficiency of NP-specific differentiation capacity and adaptability to survive the harsh microenvironment of IDD [29]. However, the hypoxic, acidic, and inflammatory IDD microenvironment can strongly restrict transplanted stem cell survival, affecting their function [30]. Current evidence suggests that pyroptosis is the inflammatory apoptosis responsible for the death of transplanted stem cells in IDD [31]. Ibuprofen, which is generally acknowledged as an anti-inflammatory inhibitor [32], may be applied to inhibit NPPC pyroptosis. However, the direct injection of Ibuprofen is easily degraded *in vivo* [33]. A conditional-responsive copolymer nano-micelles conform with the acidic IDD microenvironment can be applied for the sustained release of Ibuprofen in NPPCs. Our previous research [9] reported that the esterase activity within the transplanted stem cells increases along with the stimulation of the mildly acidic microenvironment of IDD,

suggesting that an esterase-responsive nano-micelle would be appropriate for the pre-modification of the transplanted NPPCs, promoting the efficiency of NPPCs during IDD regeneration.

Sakai et al. [34] identified tyrosine kinase receptor 2 (Tie 2) as a marker of adult mouse and human NP-tissue-derived NPPCs; consistent findings have been observed in canine and bovine notochord cells. However, these NPPCs were restricted by the limited cell source and short-term preservation [28,35,36]. They could only last 3 passages, and the percentage of the Tie2<sup>+</sup> NPPCs was only approximately  $8.66 \pm 3.94\%$ , which greatly impeded further clinical translation. To overcome these challenges, NPPCs derived from the embryo notochord are considered as potential alternatives. It is widely acknowledged that during human embryo development, the notochord forms around 22–24 days after fertilization (i.e., gestation age (GA) 3–4 weeks), which is equivalent to mouse E8.5 [37]. In the above studies, the researchers have provided a comprehensive overview of the surface marker as well as timepoint to isolate NPPCs from embryo notochord.

Herein, we report a biomaterial pre-modification strategy to pre-modify the robust long-term expandable embryo-derived NPPCs with the esterase-responsive ibuprofen copolymer nano-micelle (PEG-PIB) to promote the regeneration of IDD. PEG-PIB was endocytosed by NPPCs to form PEG-PIB pre-modified NPPCs, demonstrating the sustained release of Ibuprofen and inhibition of NPPCs pyroptosis after transplantation. Our synergistic transplantation strategy of PEG-PIB pre-modified NPPCs embodies an effective therapeutic approach to IVD functional recovery and histological regeneration, providing a novel modality for future IDD regeneration.



**Scheme 1.** General schematic of synthesis of esterase-responsive ibuprofen nano-micelles (PEG-PIB) to pre-modify embryo-derived long-term expandable nucleus pulposus progenitor cells (NPPCs) for synergistic transplantation in intervertebral disc degeneration.

## 2. Materials and methods

### 2.1. Mouse and human NPPC lines derivation and NPPC expansion medium selection

All procedures were approved by the Institutional Animal Care and Use Committee of Zhejiang University. The STOCK Tg (TIE2 GFP) 287Sato Prkdcscid/JNju mice were purchased from the Model Animal Research Center of Nanjing University. E8.5 mouse embryos were dissected from specific timed pregnant wild-type female mice (the male mouse was the STOCK Tg (TIE2 GFP) 287Sato Prkdcscid/JNju mouse), and the Tie2-GFP + embryos were handpicked under an inverted fluorescence microscope. The notochord of the embryo was isolated under an anatomic microscope (20X) and was cut, minced, and incubated in TrypLE Express Enzyme (Gibco, USA) at 37 °C for 30 min. Dissociated notochord cells were isolated using flow cytometry (FACS) (BD FACSAriaII, USA) to sort out Tie2-GFP + cells, which were considered mNPPCs. About 20,000 selected mNPPCs were equally separated into two centrifuge tubes. Half of the mNPPCs were seeded into one well of a flat-bottom 96-well plate, which was pre-coated with Matrigel (BD Matrigel™ hESC-qualified Matrix, USA) for more than 1 h as 2D culture. The other half were seeded into one well of a U-bottom low attachment 96-well plate (Gibco, USA) for 3D culture.

The 3D cultured Tie2-GFP + cells were used to select the optimal NPPC expansion medium (NPEM) culture system. The NPEM was identified by analyzing the biology of IVD development [38,39]. The primary Tie2-GFP + mNPPCs were observed and counted to obtain the optimal NPEM. Based on the Tie2-GFP + expression and proliferation rate of the mNPPCs (Fig. 1C), a cocktail of factors was identified with adding or subtracting small molecules and growth factors (Detailed methods are provided in supplementary methods). The mouse NPEM comprised a basal medium DMEM/F12 (Gibco, USA), supplemented with ascorbic acid-2-phosphate (0.5 µg/ml, Sigma), bFGF (basic Fibroblast Growth Factor, 100 ng/ml, STEMCELL technology), Y27632 (10 µM, MedChemExpress), 0.2% Heparin sodium (STEMCELL technology), CHIR99021 (10 nM, Reagents Direct), and SB202190 (1 µM, Axon Medchem). The medium was changed every other day for both 2D and 3D cultures. For passaging, cells were dissociated using TrypLE (Gibco) into single cells and passaged at 1:6–1:12 for both mNPPCs and hNPPCs every 4 or 5 days.

hNPPCs were isolated and maintained using a similar method as mNPPCs but with some modifications. Aborted human embryos of 3–6 weeks were obtained from the 2nd Affiliated Hospital of Zhejiang University (all procedures were approved by the institutional research ethics committee of Zhejiang University). The notochord was dissected and isolated under an anatomic microscope (20X). The NPEM was applied to isolate hNPPCs and GFP-mNPPCs from massive notochord cells; hNPPCs and mNPPCs that survived within the NPEM were used for further analysis [40–42]. The isolated hNPPCs were further tested using FACS to analyze their Tie2 (anti-human 334205, Biolegend) expression.

### 2.2. Characteristic of mNPPCs and hNPPCs

The Tie2-GFP + mNPPCs were cultured in both 2D and 3D formats. The 3D microspheres were observed and recorded under an inverted microscope and an inverted fluorescence microscope to screen the optimal formulation of mouse NPEM. The hNPPCs were cultured using the same NPEM conditions. After selecting the optimal NPEM, the proliferation capacities of both mNPPCs and hNPPCs were recorded after every other passage by cell counting through the automatic cell counter (Invitrogen™ Countess™ II, Gibco, USA).

To test the osteogenic, chondrogenic and adipogenic differentiation potential of the NPPCs, cultured NPPCs were seeded into a 12-well plate at a density of  $2.0 \times 10^4$  per well, and the differentiation mediums were added the day after passage. The osteogenic differentiation medium (Cyagen Biosciences, Cat. No. MUBMX-90021) was changed every 3

days for 14 days, and the characteristic mineralized nodules were examined by Alizarin Red S Staining. The chondrogenic differentiation medium consisted of DMEM supplemented with 1.25 mg/ml BSA (Bovine serum albumin, Gibco, USA),  $1 \times$  ITS, 1 mM sodium pyruvate, 0.17 mM ascorbic acid-2-phosphate, 0.35 mM proline (Sigma-Aldrich, USA), 10 ng/ml (Human) Recombinant TGF-β3 and 10 ng/ml Human Recombinant GDF-5 (PeproTech, USA). Safranin O Staining was performed after differentiation for 21 days. The adipogenic differentiation medium (Cyagen Biosciences, Cat. No. MUBMX-90031) was changed after 1 day with inducing medium A, then 3 days with maintenance medium B. After changing 5 times, the characteristic lipid droplets were examined by Oil Red O Staining.

Western Blot (WB) was performed to compare the NP specific protein expression of Collagen II (1:1000, 700 ng/ml, 28459-1-AP, Proteintech), SOX 9 (1:1000, 1095 ng/ml, ab185230, Abcam), Aggrecan (1:1000, 500 ng/ml, 3117779, Millipore), SOX 2 (1:1000, 1000 ng/ml, ab79351, Abcam), c-Myc (1:1000, 200 ng/ml, ab32072, Abcam), Oct 4 (1:1000, 1000 ng/ml, ab19857, Abcam), KLF 4 (1:1000, 1000 ng/ml, ab106629, Abcam), Brachyury (1:1000, 442 ng/ml, ab209665, Abcam), FOXA2 (1:1000, 2020 ng/ml, ab108422, Abcam), CDH 2 (1:1000, 97 ng/ml, ab76011, Abcam) and GAPDH (1:10000, 100 ng/ml, ab181602, Abcam) between mNPPCs and mESCs (hNPPCs and hiPSCs). Immunoreactivity was detected with the ECL substrate (Millipore Sigma), the relative protein level was quantified using Quantity One Software (Bio-Rad Laboratories Inc.) by densitometry. Then, the expression of CD 44 (anti-mouse/human 103011, Biolegend), CD 29 (anti-mouse 102215, anti-human 303003, Biolegend), CD 73 (anti-mouse 127219, anti-human 344015, Biolegend), CD 105 (anti-mouse 120413, anti-human 323203, Biolegend), CD 24 (anti-mouse 138505, anti-human 311105, Biolegend) was further examined as specific surface markers to distinguish mNPPCs with mESCs (hNPPCs with hiPSCs) using FACS (BD FACSCanto II, USA). In the meantime, the mNPPCs and hNPPCs were examined with immunofluorescence to assess the expression of Brachyury (1:200, 2210 ng/ml, ab209665, Abcam), FOXA2 (1:200, 10.1ug/ml, ab108422, Abcam) and NOTO (1:500, 2000 ng/ml, NBP2-83287 for mNPPCs and NBP3-17523 for hNPPCs, NOVUS).

To examine the tumorigenicity of mNPPCs and hNPPCs,  $1 \times 10^6$  cells stained with DiR (1,1-dioctadecyl-3,3,3,3-tetramethylindotricarbocyanineiodide 2.5 mg/ml, Invitrogen™, USA) were injected into the subcutaneous tissue of each BALB/cA nude mice and visualized under *in vivo* fluorescence imaging (Figs. S3C and S3D). After 1 month, all 6 mice were dissected and examined for teratoma.

### 2.3. RNA-seq and principal component analysis

Primary hNPPCs (P0) from GA 3–6 weeks human embryo notochord, hNPPCs lines at P10, and P1 human NPCs (purchased from ScienCell NO.4800) were used for RNA-seq. 3 copies were prepared for each sample and sent to LC Science for further whole transcriptome resequencing. Total RNA was extracted from the above three groups using RNAiso reagent (Takara, Japan) according to the manufacturer's protocol. The cDNA libraries were gathered using the mRNA-seq sample preparation kit (Illumina, CA). The paired-end sequencing was performed on an Illumina Hiseq 4000 (LC Science, China) following the recommended protocols. StringTie was used to measure the expression of mRNAs by calculating the FPKM using GRCh38 as the reference genes. Cultured hNPPCs (P10) were used as control. Differentially expressed mRNAs were identified using the criteria:  $\log_2$  (fold change)  $> 1$  or  $\log_2$  (fold change)  $< -1$  and  $p < 0.05$  using the R package Ballgown. The heatmap was generated in R using the pheatmap package.

### 2.4. Nucleus pulposus differentiative potential

2 million NPPCs (both mNPPCs and hNPPCs) were counted and equally seeded into 10 wells of a 96-well U-bottom plate (each with 200 thousand cells) with NPEM for further differentiation. The NP-specific

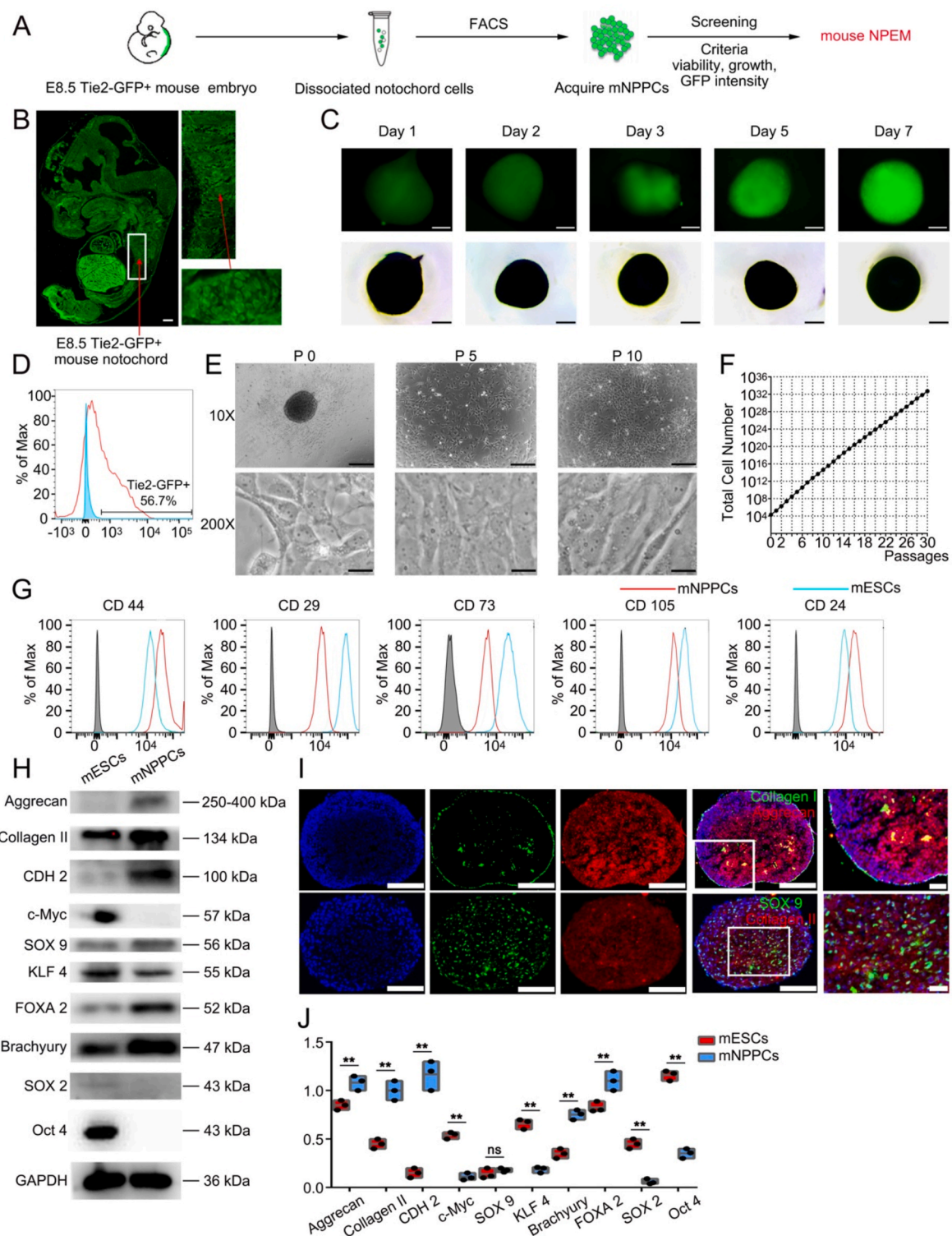


**Fig. 1.** Isolation and characterization of *Tie2*<sup>+</sup> mouse embryo derived mNPPCs *in vitro*. (A) Schematic diagram showing the isolation of E8.5 *S Tie2-GFP*<sup>+</sup> mouse embryo derived mNPPCs and screening of mouse NPEM. (B) The GFP epifluorescence images of the E8.5 *Tie2-GFP*<sup>+</sup> mice embryo on the left. Detailed images of notochord (white rectangle) and is further amplified (red arrow). Scale bar = 100  $\mu$ m. (C) Bright field (bottom row) and GFP epifluorescence (up row) images of culture mNPPCs aggregates at the Day1, 2, 3, 5, 7 after cultured in 3D format. Scale bar = 500 $\mu$ m. (D) The FACS results of isolation *Tie2-GFP*<sup>+</sup> cells from the dissociated notochord cells. (E) Bright field 10X images of cultured mNPPCs from embryos at different passages. Scale bar = 100  $\mu$ m. Bright field 200X images of cultured mNPPCs from embryos at different passages. Scale bar = 2000  $\mu$ m (F) Number of mNPPCs after 30 passages (starting from  $2 \times 10^4$  cells). (G) FACS analysis of indicated surface markers on mNPPCs (red line) compared with mESCs (blue line). The grey column indicated the IgG for each antibody. (H) Western blot analysis of indicated proteins between mESCs and mNPPCs. (I) Immunofluorescence results (20X) of mNPPCs with Aggrecan, Collagen II, Collagen I and SOX9 expression. Scale bar = 100  $\mu$ m (J) The quantitative result of Fig. 1H. \*\**p* < 0.01, \**p* < 0.05 vs. mESCs (Student's *t*-test).

differentiation medium was changed the second day after seeding and continuously switched every 2 days for 21 days. 4 of the microspheres were fixed with 4% paraformaldehyde and frozen sectioned for immunofluorescence, and the remaining 6 were equally separated for RT-PCR and WB assays.

The NP-specific differentiation medium for NPPCs was carried out as previously described with some modifications [43], which consisted of DMEM supplemented with 1.25 mg/ml BSA (Gibco, USA),  $1 \times$  Insulin-Transferrin-Selenium (ITS), 0.1  $\mu$ M dexamethasone, 1 mM sodium pyruvate, 0.17 mM ascorbic acid-2-phosphate, 0.35 mM proline (Sigma-Aldrich, USA), 10 ng/ml Transforming Growth Factor- $\beta$ 1 (TGF- $\beta$ 1), 10 ng/ml Growth Differentiation Factor 5 (GDF-5) and 2 ng/ml Bone Morphogenetic Protein (BMP-2) (PeproTech, USA).

The NP-specific differentiation capacity of mNPPCs was compared with mESCs and mBMSCs using RT-PCR (hNPPCs were compared with hiPSCs and hADSC). The NP-specific differentiation media for MSCs [12] and PSCs [23] used were mentioned in our previous research. The relative protein expression for Collagen II (1:1000, 700 ng/ml, 28459-1-AP, Proteintech), SOX 9 (1:1000, 1095 ng/ml, ab185230, Abcam), Aggrecan (1:1000, 500 ng/ml, 3117779, Millipore), KRT 19 (Keratin 19, 1:1000, 1000 ng/ml, 12434s, Cell Signaling Technology) was examined using WB.

The relative mRNA expression for several markers (ACAN, COL2A1, SOX9, COL1A1 and KRT19) was measured by RT-PCR, and 18s was used as the reference gene. Their CT values were mESCs' 18s CT =  $30.2 \pm 0.5$ , mBMSCs' 18s CT =  $29.9 \pm 0.2$ , mNPPCs' 18s CT =  $30.4 \pm 0.8$  (with hiPSCs' 18s CT =  $28.8 \pm 0.2$ , hADSCs' 18s CT =  $29.4 \pm 0.7$ , hNPPCs' 18s CT =  $28.7 \pm 0.3$ ). All primers were synthesized by Sangon Biotech (Shanghai, China) (Table S1). The expression level of relative gene expression was calculated by the  $2^{-\Delta\Delta CT}$  method.

## 2.5. Adaptation with IDD microenvironment

The *in vivo* adaptability of mNPPCs in the IDD microenvironment was compared with mESCs and mBMSCs (hNPPCs were compared with hiPSCs and hADSC). All cells were prepared with DiR (2.5 mg/ml, Invitrogen™, USA). 12 female SD rats were divided into two groups after successfully establishing the IDD model (the detailed method is stated in 2.16); 6 were injected with 10 thousand mESCs, mNPPCs and mBMSCs each. The remaining 6 were injected with 10 thousand hiPSCs, hNPPCs and hADSCs each. All rats were examined with *in vivo* fluorescence imaging system to assess the viability of each kind of cell.

To simulate the *in vivo* IDD microenvironment, mESCs, mNPPCs, mBMSCs, hiPSCs, hNPPCs and hADSCs were cultured with 4 factors, in the pH 6.2 cultural medium, with 10 mg/mL IL-1 $\beta$  induced inflammatory circumstances, in a tri-gas incubator with an oxygen concentration of 2% and the combination of all three factors. After culturing for 24 h, all cells underwent apoptosis detection.

## 2.6. Preparation of materials for micelle synthesis

Ibuprofen, 2-hydroxyethyl methacrylate (HEMA), 1-(3-Dimethylaminopropyl)-3-ethylcarbodiimide hydrochloride (EDC), 4-dimethylaminopyridine (DMAP), 2-Hydroxy-2-methylpropionophenone and 2,2'-azobis(2-methylpropionitrile) (AIBN) were purchased from Energy Chemical (Shanghai, China).

## 2.7. Synthesis of the monomer 2-(methacryloyloxy) ethylibuprofen (HIB)

A mixture of Ibuprofen (2 g, 9.7 mmol), HEMA (1.5 g, 11.5 mmol), and DMAP (0.24 g, 2.0 mmol) was dissolved in 20 mL of DCM. A solution of EDC (2.78 g, 14.5 mmol) in DCM (30 mL) was added to the solution at 0 °C, and the mixture was stirred at room temperature for 12 h. The crude product was washed with 1 M HCl three times. The product was purified by column chromatography. The <sup>1</sup>H NMR spectral data of the product was as follows: <sup>1</sup>H NMR (400 MHz, CDCl<sub>3</sub>)  $\delta$  = 7.19 (d, J = 8.1,

2H), 7.07 (d, J = 8.1, 2H), 6.03 (s, 1H), 5.56–5.50 (m, 1H), 4.35–4.25 (m, 4H), 3.72 (q, J = 7.2, 1H), 2.43 (d, J = 7.2, 2H), 1.88 (dd, J = 4.9, 3.6, 3H), 1.82 (dd, J = 13.5, 6.8, 1H), 1.49 (d, J = 7.2, 3H), 0.89 (d, J = 6.6, 6H).

## 2.8. Synthesis of block copolymer poly (ethyleneglycol) – poly [2-(methacryloyl) ethylibuprofen] (PEG-PIB)

The macromolecular chain transfer agent (PEG-PETTC) was prepared according to the literature [44]. PEG-PIB was synthesized via RAFT polymerization. First of all, CTA (0.20 g, 0.04 mmol), HIB (0.20 g, 0.6 mmol), AIBN (3.3 mg, 0.02 mmol), and DMF (2 mL) were charged into a Schlenk tube fitted with a magnet. The solution was degassed by purging with nitrogen (N<sub>2</sub>) for 30 min. The polymerization was carried out at 70 °C for 15 h. The mixture was precipitated in diethyl ether three times to obtain the block polymer PEG-PIB as a white powder. The <sup>1</sup>H NMR spectral data of the product was as follows: <sup>1</sup>H NMR (400 MHz, DMSO)  $\delta$  = 7.15 (22.85H), 7.02 (22.05H), 4.14 (42.02H), 3.73-3.65 (10.43H), 3.51 (454H), 2.32 (22.79H), 1.74–1.68 (11.70H), 1.41–1.24 (33.09H), 0.78 (67.37H).

## 2.9. Preparation and characterization of the micelle

The size and morphology of the PEG-PIB micelles were characterized by a dynamic light scattering (DLS) spectrometer (Nano series ZEN3600, Malvern Instruments Ltd., UK) and a transmission electron microscope (TEM) (JEM-1200EX, Japan).

The micelle solution (10 mg/mL) was prepared and mixed with PBS of different pH values (6.2, 6.4, 6.8, 7.4) adjusted with hydrochloric acid. The mixture was incubated at 37 °C and tested at fixed intervals using DLS. The Z-average diameters from every test were recorded and plotted as a function of time.

## 2.10. Esterase degradation rate of PEG-PIB

The 10 mg/ml PEG-PIB were dissolved in PBS and subdivided into a pH7.4 without esterase group and different pH (6.2, 6.4, 6.8, 7.4) with esterase (220 U/mL) groups. A nanoparticle solution for each group (1 mL, containing 10 mg polymer) and esterase were sealed in a dialysis bag with a molecular weight cut off at 3500 Da and dialyzed in 37 mL of PBS with 2% Tween 80. 200  $\mu$ L of the solution was withdrawn from the bag for HPLC analysis at predetermined intervals (0, 1, 2, 4, 8, 12, 24, 48, and 72 h).

## 2.11. PEG-PIB biocompatibility

The PEG-PIB (10 mg/ml) was incubated with hNPPCs for endocytosis. The culture supernatant was taken at 1, 3, 5 and 7 days for CCK-8 assay to assess the cell proliferation capacity of PEG-PIB endocytosed hNPPCs. Meanwhile, rhodamine was packaged within the PEG-PIB through dialysis and FACS were used to assess successful endocytosis. Then, FDA (Sigma-Aldrich) was dissolved in DMSO at 10 mg/mL as a stock solution and diluted by PBS to 1 mg/mL as a working solution. For fluorescence imaging of esterase activity, FDA was added at a final concentration of 5  $\mu$ g/mL and incubated with the cells for 30 min before observation, as previously described. The rhodamine-loaded PEG-PIB (10 mg/ml) was added to NPDM of different pH (6.2, 6.4, 6.8, and 7.4) and incubated at 37 °C for 10min to observe the endocytosis and degeneration of the PEG-PIB. The images were observed using a fluorescence microscope (Leica).

## 2.12. Degradation rate of PEG-PIB in hNPPCs

The PEG-PIB were incubated with the hNPPCs and subdivided into NPDM groups of different pH (6.2, 6.4, 6.8, and 7.4). At each time point, the hNPPCs were washed with PBS three times and lysed to collect the

supernate to obtain the degradation product of PEG-PIB. 200  $\mu$ L of the supernate was withdrawn from the bag for HPLC analysis at pre-determined intervals (0, 1, 2, 4, 8, 12, 24, 48, and 72 h).

### 2.13. Pyroptosis in degenerated IVDs

The samples of degenerated nucleus pulposus were obtained from lumbar disc herniation patients; the samples of normal nucleus pulposus were obtained from the scoliosis patients (all procedures were approved by the institutional research ethics committee of Zhejiang University). The samples were paraffin-embedded, and sections were obtained. Immunohistochemistry was used to assess apoptosis-associated speck-like protein containing a CARD (ASC) (1:200, 8285 ng/ml, PA5-120131, Thermo Fisher Scientific) protein expression in degenerated IVDs, which is considered a marker of pyroptosis [45].

Primary hNPCs and primary degenerated hNPCs (hDNPCs) were isolated from the degenerated nucleus pulposus samples. RNA and protein were extracted from primary cells to assess gene and protein expression differences in pyroptosis. RT-PCR was performed using the same protocol as above to quantify the expression of IL-1 $\beta$ , ASC, NLRP3 and CASPASE1 as the pyroptosis representative genes between DNPCs and NPCs. Western blot assays were performed to assess the difference in protein expression of IL-1 $\beta$  (1:1000, 12703s, 1000 ng/ml, Cell Signaling Technology), ASC (1:1000, 1000 ng/ml, 13883s, Cell Signaling Technology), NLRP3 (1:1000, 1000 ng/ml, 15101s, Cell Signaling Technology) and Caspase1 (1:1000, 1000 ng/ml, 24232s, Cell Signaling Technology) between DNPCs and NPCs.

### 2.14. Pyroptosis of hNPPCs in vitro

Hydrochloric acid was added to the NPDM to stimulate a severe IDD microenvironment, both the control group and pH 6.2 group hNPPCs were washed 3 times with ddH<sub>2</sub>O, and their cell membranes were lysed with 0.3% Triton X-100. Then, the samples were incubated with 5% BSA at 37 °C for 1 h and incubated overnight at 4 °C with the appropriate primary antibody ASC (1:1000, 1000 ng/ml, 13883s, Cell Signaling Technology), followed by incubation with the appropriate secondary antibody conjugated to FITC (1:500). The microspheres were observed under a fluorescence microscope.

### 2.15. PEG-PIB inhibits hNPPCs pyroptosis in vitro

After hNPPCs were pre-modified with PEG-PIB, the live/dead viability assay kit (Us Everbright, China) was used to conduct Live/dead assays of PEG-PIB pre-modified hNPPCs at different pH values (6.2, 6.4, 6.8, and 7.4). Meanwhile, IF was used to examine pyroptosis-associated ASC expression within the rhodamine packaged PEG-PIB hNPPCs at different pH values (6.2, 6.4, 6.8, and 7.4) after co-culture for 24 h.

Then WB was used to assess the possible pathways underlying the inhibitory effect of PEG-PIB on hNPPCs pyroptosis. Groups were set as follows: the normal control (NC) group did not undergo treatment with acid stimulation and PEG-PIB; for the degeneration control (DC) group, the medium was adjusted to 6.2, and the PEG-PIB group was treated with acidic stimulation and PEG-PIB. All groups underwent Western blot analysis to quantify the nucleoprotein expression of NLRP3, ASC, Caspase1, IL-1 $\beta$ , I $\kappa$ B $\alpha$  (1:1000, ab10286, Abcam) and p-I $\kappa$ B $\alpha$  (1:1000, 2859T, Cell Signaling Technology) to identify the functional pathways associated with PEG-PIB.

### 2.16. Animal procedure

SD rats (250 g) were purchased from the Zhejiang Chinese Medical University Laboratory Animal Research Center. The surgical procedure was conducted as described in our previous studies [23]. Briefly, 3% pentobarbital sodium was injected intraperitoneally as the anesthetic after coccygeal vertebrae Co7/Co8 and Co8/Co9 were localized using

digital palpation and double-checked by a trial radiograph. A sterile 20-gauge needle (outer diameter 0.91 mm) was inserted just through the AF into the middle of the NP. The needle was rotated 360° and held for 30 s. 80 male SD rats were divided into five groups: the normal control (NC) group (without needle puncture or DMEM injection), the degeneration control (DC) group (needle puncture after 2 weeks and then injected with DMEM injection), the PB group (needle puncture after 2 weeks and then injected with PEG-PIB), the NPPC group (needle puncture after 2 weeks and then injected with hNPPCs) and the PB-NPPC group (needle puncture after 2 weeks and then injected with PEG-PIB modified hNPPCs).

### 2.17. Disc height measurement

After injection for 2, 6, 10 and 18 weeks, caudal disc radiographs were taken at each time point by the molybdenum target radiographic imaging unit (GE Mammography DMR Bucky 18 × 24, UK) to examine the disc height of each group. All rats were anesthetized and placed supine, ensuring their tails were completely unstressed and straight. The digital images were obtained by a skilled observer. The disc height index (DHI) is a relative value obtained by dividing the average height of a single intervertebral disc by the average of two adjacent caudal discs. The DHI% is further divided with NC group's DHI at each time point. (Fig. 5B). The relative height was calculated using ImageJ software (NIH, Bethesda, USA) by three blinded observers.

### 2.18. MRI procedure and data processing

T2-weighted sections in the sagittal and transverse planes were taken by a 3.0-T MRI (GE Medical Systems, UK) to investigate the water content and the structure of the caudal spine at 2, 6, 10 and 18 weeks after modeling. All anesthetized rats were placed supine to keep their tails straight. The parameters of the MRI were as follows: echo time, 80 ms; spin-echo repetition time, 2275 ms; field of view, 5 cm; number of excitations, 8; slice thickness, 1.5 mm; and no phase wrap. The images were processed using the GE ADW4.2 workstation, and the water content of the NP was evaluated by the MRI index. The index was measured by three investigators in an independent and blinded fashion. Finally, alterations of NP were evaluated by the Pfirrmann grading system.

The rats were sacrificed by intraperitoneal injections of pentobarbital sodium (150 mg/kg), and the caudal spine samples were washed with ultrapure water, then dipped in 4% paraformaldehyde for 3 days. After decalcification with 10% EDTA for 2 months, the specimens were embedded with paraffin and cross-sectioned (4  $\mu$ m). The samples were stained using hematoxylin and eosin (H&E) and Safranin O-Fast Green (S–O). The morphology and cellularity of the IVDs were evaluated by three investigators independently using the latest grading scale (Table S4) [46].

### 2.19. Immunohistochemistry

After being deparaffinized in xylene, the specimens were rehydrated and treated with 3% H<sub>2</sub>O<sub>2</sub> for 15 min. Then, the specimens were blocked with 5% Bovine Serum Albumin (BSA) for 30 min at RT and incubated at 4 °C overnight with the Collagen II antibody (1:200, 5000 ng/ml, ab34712, Abcam) and Aggrecan antibody (1:200, 5000 ng/ml, ab216965, Abcam). After washing with PBS 3 times, the specimens were incubated at 37 °C for 30 min with biotin-labeled rabbit anti-mouse IgG (1:200), and the staining was detected by the streptavidin-biotin complex (SABC) method.

### 2.20. Immunofluorescence

For immunofluorescence detection, all samples were washed 3 times with ddH<sub>2</sub>O, and their cell membranes were lysed with 0.3% Triton X-100. Then, the samples were incubated with 5% BSA at 37 °C for 1 h and

incubated overnight at 4 °C with the appropriate primary ASC antibody (1:200, 5000 ng/ml, 13883s, Cell Signaling Technology), followed by incubation with the appropriate secondary antibody conjugated to FITC (1:500). The microspheres were finally observed under a fluorescence microscope.

### 2.21. Modulus of elasticity of IVDs

The elasticity modulus was measured by the electronic type universal testing machine (Instron 5944 SingleColumn Tabletop Testing System, Instron, USA). At least two vertebral bodies were preserved for testing. The muscles on the vertebral were removed as cleanly as possible and the upper and lower vertebral were tightly clipped in the two clamps of the machine (Fig. 7F), the compression speed was set to 0.1 mm/s.

### 2.22. Statistical analyses

The data are shown as the mean  $\pm$  standard deviation (SD). All data was subject to outlier (ROUT method) and normality (Shapiro-Wilk) testing. Parametric, normal datasets were analyzed using the Student's t-test and ANOVA test with post-hoc Tukey's testing. We would like to mention that we use Student's t-test to analyze the different protein expression between mESCs and mNPPCs (hiPSCs and hNPPCs) (Figs. 1J and 2I), CCK-8 results of the PEG-PIB effect on hNPPCs proliferation (Fig. 3L), ASC expression in hNPPCs treat with different pH values (Fig. 4G) etc. One-way ANOVA test to analyze the  $\zeta$ -potential of PEG-PIB at different pH values (Fig. 3G), the endocytosis efficiency of PEG-PIB at different pH values (Fig. 3K), the percentage of living hNPPCs at different pH circumstance (Fig. 4H), the ASC expression in rhodamine packaged PEG-PIB pre-modified hNPPCs at different pH circumstance (Fig. 4I), the proliferation potential of PEG-PIB pre-modified hNPPCs at

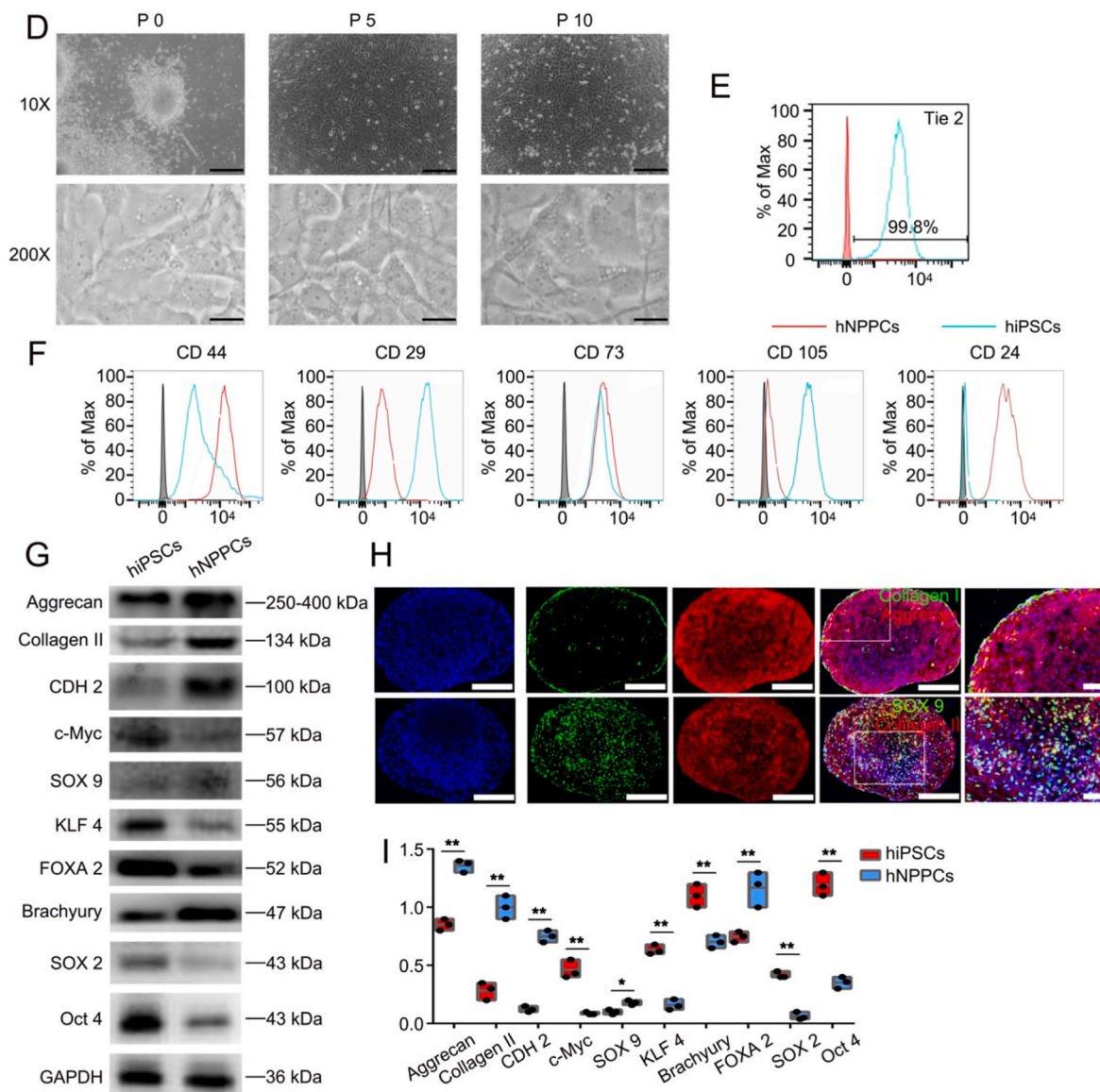


**Fig. 2.** Derivation and long-term culture of embryo derived hNPPCs. (A) Schematic diagram showing the isolation of human embryo derived hNPPCs. (B) The total embryo dissected and their gestation ages as well as the derivation efficiency. (C) Number of hNPPCs after 30 passages (starting from  $5.4 \times 10^5$  cells). (D) Bright field 10X images of cultured mNPPCs from embryos at different passages. Scale bar = 100  $\mu$ m. Bright field 200X images of cultured mNPPCs from embryos at different passages. Scale bar = 2000  $\mu$ m (E) FACS analysis of hNPPCs' expression of Tie2. (F) FACS analysis of indicated surface markers on hNPPCs (red line) compared with hiPSCs (blue line). The grey column indicated the IgG for each antibody. (G) Western blot analysis of indicated proteins between hiPSCs and hNPPCs. (H) Immunofluorescence results (20X) of hNPPCs with Aggrecan, Collagen II, Collagen I and SOX9 expression. Scale bar = 100  $\mu$ m. (I) The quantitative result of Fig. 2G. \*\*p < 0.01, \*p < 0.05 vs. hiPSCs. (Student's t-test).

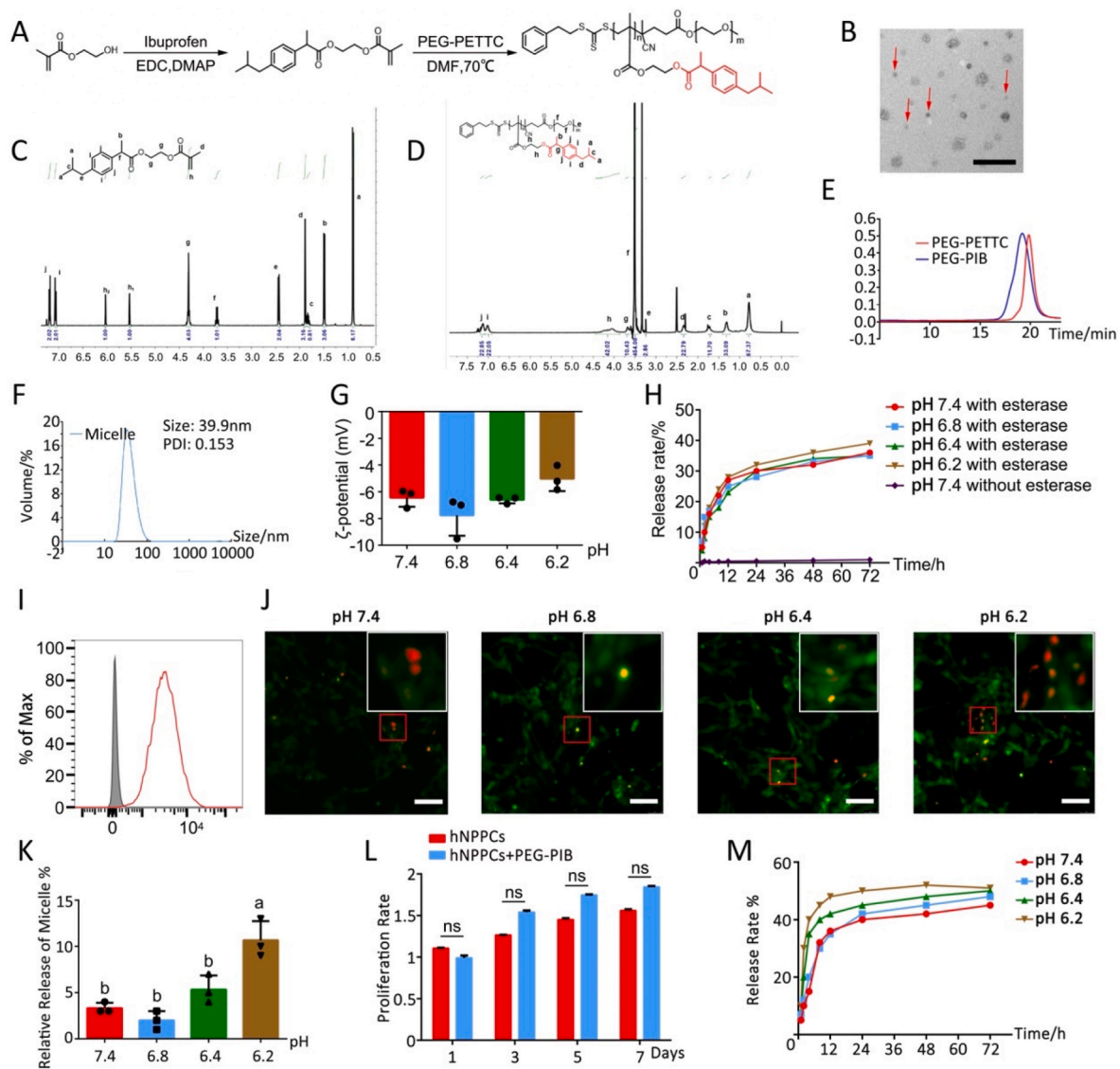


**Fig. 3.** Synthesis and characterization of PEG-PIB (A) Synthesis diagram of PEG-PIB. (B) SEM results of PEG-PIB (red arrow). Scale bar = 100  $\mu\text{m}$  (C)  $^1\text{H}$  NMR spectrum of PEG-PIB monomer. (D)  $^1\text{H}$  NMR spectrum of PEG-PIB polymeride. (E) GPC traces of the PEG-PETTC and PEG-PIB. (F) Size distributions and the PDI of PEG-PIB. (G)  $\zeta$ -potential of PEG-PIB at different pH values.  $p < 0.05$  (one-way ANOVA test) (H) ibuprofen release rate from PEG-PIB with or without esterase at different pH values (pH 7.4, pH 6.8, pH 6.4, pH 6.2).  $p < 0.05$  (two-way ANOVA test) (I) FACS results of rhodamine packaged PEG-PIB endocytosed by the hNPPCs. (J) Immunofluorescence results of hNPPCs treated with FDA at different pH values (pH 7.4, pH 6.8, pH 6.4, pH 6.2), and further added rhodamine packaged PEG-PIB for 30 min to observe the efficiency of endocytosis. Scale bar = 50  $\mu\text{m}$  (K) The quantitative result of Fig. 3J  $p < 0.05$  (one-way ANOVA test) (L) CCK-8 results of the PEG-PIB effect on hNPPCs proliferation. (Student's  $t$ -test) (M) ibuprofen release rate from PEG-PIB within the hNPPCs at different pH values (pH 7.4, pH 6.8, pH 6.4, pH 6.2).  $p < 0.05$  (two-way ANOVA test).

different pH circumstance (Fig. 4J); the pyroptosis related different protein expression (Fig. 4L); the histological scores of all five groups at 18 weeks after modeling (Fig. 7B) etc. Two-way ANOVA test is used to analyze the Ibuprofen release rate from PEG-PIB with or without esterase at different pH values (Fig. 3H); the Ibuprofen release rate from PEG-PIB within the hNPPCs at different pH values (Fig. 3M); the disc height changes (Fig. 5C), the T2 MRI index of each group (Fig. 5E and F) etc. Detailed regression analyses are annotated with the figure legends. All statistical analyses were performed using SPSS software (SPSS Inc., USA). The significance threshold was set at a  $p$  value  $< 0.05$ .

### 3. Results and discussion

#### 3.1. Isolation and characterization of NPPCs

Over the years, stem cells termed NPPCs have been isolated from the

adult IVD tissues in rats, pigs and other species [24–27]. These adult IVD-derived NPPCs have been established to possess stem cell-like characteristics with high efficiency of NP-specific differentiation and good adaptability to harsh IDD microenvironment. However, the source and proliferation problems of NPPCs strongly impede further clinical translation.

To provide a better cell source of NPPCs, long-term expandable mNPPCs were obtained from the E8.5 Tie2-GFP + mice embryo notochord (Fig. 1A). The embryo notochord was dissected and digested into single cells, and a fluorescence-activated cell sorter (FACS) was used to gather the Tie2-GFP + mNPPCs (Fig. 1D). The GFP-mNPPCs and hNPPCs were isolated using a similar protocol (Fig. 2A), without FACS but using NPEM to screen NPPCs. Both flat cultured P0 NPPCs were seeded into the 96-well plate, and typical progenitor cell colonies were observed. The NPPCs were then transferred into the 12-well plate, where we observed that the mNPPCs were smaller in size than hNPPCs; both

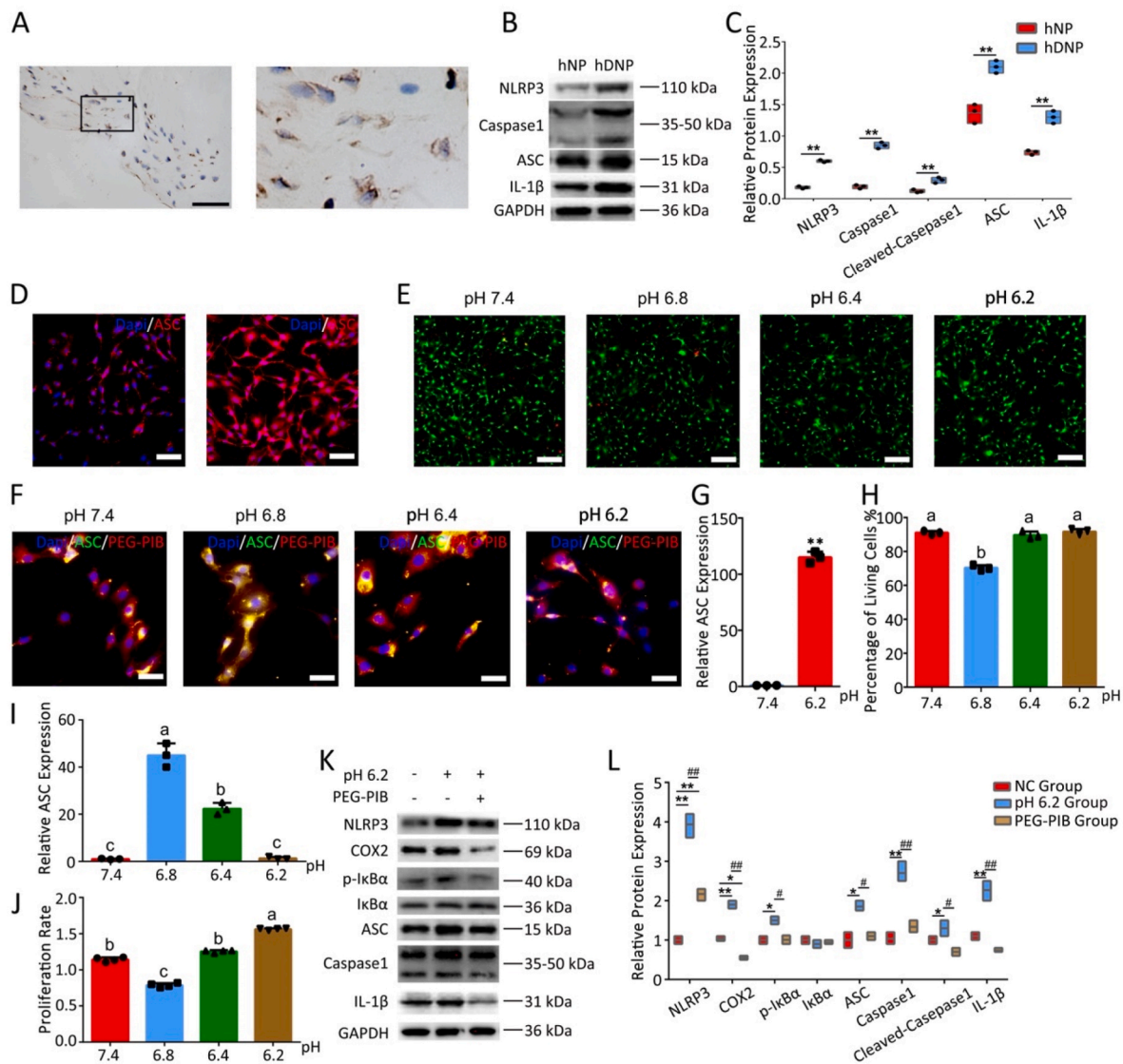


**Fig. 4.** PEG-PIB inhibit hNPPCs pyroptosis *in vitro* (A) IHC results of ASC expression from clinical degenerated IVD sample. (B) Western blot analysis of indicated proteins between hNP and hDNP. (C) The quantitative analysis of Fig. 4B.  $**p < 0.01$ ,  $*p < 0.05$  vs. hNP. (Student's t-test) (D) Immunofluorescence results of ASC expression in hNPPCs treat with different pH values (pH 7.4 and pH 6.2) (E) Fluorescence image of live (green) and dead (red) cells at different pH circumstance (pH 7.4, pH 6.8, pH 6.4, pH 6.2). Scale bar = 100  $\mu$ m (F) Immunofluorescence of ASC expression in rhodamine packaged PEG-PIB pre-modified hNPPCs at different pH circumstance (pH 7.4, pH 6.8, pH 6.4, pH 6.2). Scale bar = 100  $\mu$ m (G) The quantitative analysis of Fig. 4D.  $**p < 0.01$  vs. pH 7.4. (Student's t-test) (H) The quantitative analysis of Fig. 4E  $p < 0.05$  (one-way ANOVA test) (I) The quantitative analysis of Fig. 4F  $p < 0.05$  (one-way ANOVA test) (J) CCK-8 results of the proliferative potential of PEG-PIB pre-modified hNPPCs at different pH circumstance (pH 7.4, pH 6.8, pH 6.4, pH 6.2).  $p < 0.05$  (one-way ANOVA test) (K) Western blot analysis of indicated proteins between all 3 groups (NC group, pH 6.2 group and PEG-PIB group). (L) The quantitative result of Fig. 4K.  $**p < 0.01$ ,  $*p < 0.05$  vs. NC group.  $##p < 0.01$ ,  $#p < 0.05$ , vs. PEG-PIB group. (one-way ANOVA test).

maintained an immature fibroblast-like morphology and typical fragmented vacuoles were observed at each passage in both mNPPCs and hNPPCs (Figs. 1E and 2D). Although Rodrigues-Pinto et al. [47] indicated the undetectable of Tie2 on human embryo notochord immunostainings, Sakai et al. [34] later showed that Tie2 was present in human embryo notochord via immunostainings and FACS. Herein, we have also exhibit positive Tie2 expression in hNPPCs (Fig. 2E), which is consistent with Sakai et al.'s results. To prove that our embryo-derived NPPCs were not embryonic stem cells (ESCs), we used FACS and Western blot to distinguish mNPPCs from mESCs (hNPPCs were compared with the human-induced pluripotent stem cells (hiPSCs)). The mNPPCs exhibited higher expression of CD44 and CD24 and lower expression of CD29, CD73 and CD105 than the mESCs (Fig. 1G). The hNPPCs showed slightly different results than the mNPPCs, with no significant difference in CD73 expression between hNPPCs and hiPSCs (Fig. 2E). Meanwhile, the

expression of NP-specific protein (Collagen II, Aggrecan and SOX 9) in mNPPCs was higher than in the mESCs. On the contrary, the expression of the pluripotency-related proteins (SOX 2, c-Myc, Oct 4 and KLF 4) in mNPPCs was significantly lower than in the mESCs (Fig. 1H and I). The results for hNPPCs and hiPSCs were comparable (Fig. 2F and G). Both NPPCs retained the potential to differentiate and participate in osteogenesis, chondrogenesis and adipogenesis (Figs. S4A and S4B). In the meantime, their NP-specific differentiation capacity was further assessed using immunofluorescence assays (Figs. 1J and 2H). The 3D cultured NPPC microspheres expressed high levels of homogeneous Collagen II and Aggrecan, which are the defining main ECM of NP cells (NPCs) with Collagen I localized on the edge of the pallets. Almost half of the cells expressed typical cartilage-related SOX 9, also considered a nuclear localization marker of NPCs.

The NP-EM enabled the passage of mNPPCs and hNPPCs for over 30

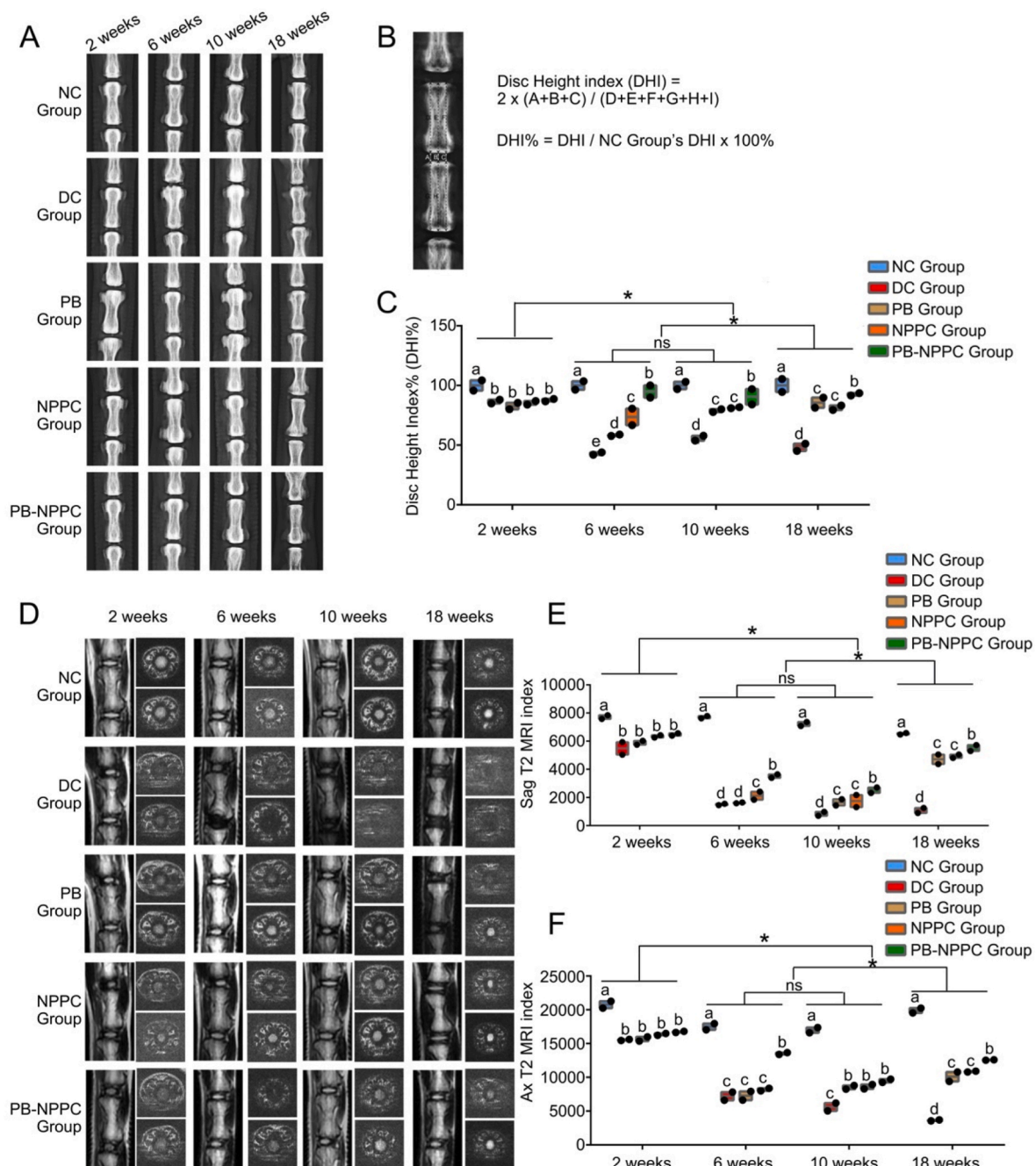


**Fig. 5.** Radiographs and MRI results. (A) Radiographs of all five groups, which were obtained at 2, 6, 10 and 18 weeks after modeling, both IVD segments were treated with the same procedure. (B) DHI% was calculated from digitized radiographs using Image J. (C) The quantitative analysis of DHI%. \* $p < 0.05$ . (two-way ANOVA test) (D) Representative T2 MRI scans, both IVD segments were treated with the same procedure. (E) The sagittal plane T2 MRI index of each group. \* $p < 0.05$  (two-way ANOVA test) (F) The transverse plane T2 MRI indexes of different groups. \* $p < 0.05$  (two-way ANOVA test).

generations at an extremely high rate (Figs. 1F and 2C) without losing their proliferation and differentiation capacity. bFGF was used to promote the proliferation of NPPCs, and Y27632 was added to inhibit the Rho-Rock signaling pathway to weaken the formation of NPPCs colonies while maintaining their differentiation potential. CHIR99021 was given to inhibit the function of TGF- $\beta$  and prevent differentiation of NPPCs, and SB202190 (p38 inhibitor) was provided to maintain the progenitor status of NPPCs. All microspheres were observed under an inverted fluorescence microscope daily with different media combinations. Importantly, the hNPPCs exhibited relatively slower growth, suggesting there might be different pathways between mNPPCs and hNPPCs, warranting further study.

The RNA-sequencing (RNA-seq) analysis of human NPCs (P1), primary hNPPCs (GA 3–6 weeks) and cultured hNPPCs (P10) revealed 8321 differentially expressed genes. These differences were subsequently used as the NPPC signature in further analyses (Table S2). Principal component analysis (PCA) of NPPC genetic signature revealed that primary hNPPCs were closely related, indicating a primary hNPPC signature. However, the human NPCs showed a significant batch effect, with one of the hNPCs significantly different from the remaining two during PCA. Interestingly, all three cultured hNPPCs clustered together, which were closer to the primary hNPPCs than the human NPCs (both PC1 and PC2 axes) (Fig. 2H). NPPC markers such as TIE2 (TEK), GD 2 (GDAP 2), COL2A1, CD24, and SOX9 exhibited similar expression levels between

primary hNPPCs and cultured hNPPCs, which was significantly lower in the human NPCs. Other NPPC markers, like NOTO, FOXJ 1, FOXA 1, FOXA 2, SHH, SOX 5, SOX 6 and KRT 19, exhibited significantly higher expression in the primary hNPPCs than the cultured hNPPCs as well as the human NPCs. In contrast, the expression of TGF $\beta$  3, TGF $\beta$  1, GDF 5, PAX 1, ACAN and PRG 4 was significantly lower in primary hNPPCs and cultured hNPPCs (Fig. S2D). These results indicated that the notochord relevant gene expression of NPPCs was preserved with NPEM and like many other tissue-specific progenitor cells, the NPPCs exhibited a NP-specific differentiation potential by sharing a similar NP relevant gene expression with human NPCs.

We further examined the NP-specific differentiation potential and IDD microenvironment adaptability of NPPCs compared with MSCs and PSCs. mNPPCs exhibit a significant higher gene and protein expression in Collagen II, Aggrecan and KRT 19 compared with mESCs and mBMSCs, their relative protein expression of SOX9 showed no significant difference which is quite opposite with gene expression. hNPPCs are compared with hiPSCs and hADSCs. Different results indicated that hNPPCs showed no significant difference in Collagen II and Aggrecan protein expression compared with hADSCs, the SOX9 gene expression indicated no significant difference between all three cells. (Fig. S4). The adaptability of NPPCs exhibit much better than PSCs and MSCs both *in vivo* and *in vitro*. Based on the data analysis, we have some hypothesis with the NPPCs' well function. Firstly, the NPPCs originated from the notochord tissue itself were supposed to have a better adaptability in the degenerated IVD niches. Evidence suggests that the notochord cells retain a better morphologic phenotype within the serum-free culture media [48], which is consistent with the NPEM. Secondly, our preliminary RNA-seq data analysis showed that the NPPCs shared almost the same group of highly expressed genes with the notochord cells. Meanwhile, after passage 10 times with NPEM, both mNPPCs and hNPPCs still possessed the typical but fragmented notochord vacuole, indicating preservation of the notochord phenotype. The injection of notochord-like NPPCs could efficiently restore the number of NPCs and regain the function of IVDs. Last but not the least, there is evidence of exogenous human MSCs migrated through bovine *ex vivo* IVD endplate, the migration of MSCs was enhanced in IVDs cultured under degeneration-inducing conditions by releasing chemoattractive molecules to recruit exogenous cells [49–51]. Another research in IVDs from several species including human, has demonstrated the possible progenitors existed in nucleus pulposus and annulus fibrosus [52]. However, despite the presence of the exogenous-cell migration system, the *in vivo* lack of vascular access strongly restricts the migration from other regions [53,54]. Therefore, we assume that the injection of NPPCs could probably accelerate the migration of residual progenitors in IVD niches.

However, there are still many problems restrict the clinical translation of NPPCs. First of all, the use of Matrigel is a complex mixture of ECM proteins which is extracted from animal tumor tissue. Despite the outstanding bioactivity, the isolation from tumor tissue hinders its translation into clinical applications. Kim et al. [55] has demonstrated that the extracellular matrix hydrogels derived from decellularized gastrointestinal tissues are effective alternatives to the current gold standard, Matrigel. This might be a solution to avoid Matrigel's prohibition in clinical translation, which needs further experiment. Moreover, the source of aborted human embryos is limited. Ideally, hNPPCs derived from the hiPSCs represent a better approach to obtaining hNPPCs. Many studies have been conducted to acquire iPSCs-derived nephrogenic progenitors [40], chondroprogenitors [56], and hematopoietic progenitor cells [57] etc. In our previous study, we hypothesized that NPPCs could differentiate from iPSCs [58] and documented the differentiation protocol of hiPSCs differentiation into hNPCs [23]. Our future studies will focus on isolating hNPPCs during the differentiation process at the optimal time point to acquire hiPSC-hNPPCs.

Overall, we provide a promising cell source for IDD transplantation. Our embryo-derived NPPC lines exhibit the advantages of simple acquisition, fast proliferation, NP-specific differentiation potential and

IDD microenvironment adaptability. These NPPCs offer an efficient application platform for further IDD treatment.

### 3.2. Synthesis and characterization of PEG-PIB nano-micelle

The mildly acidic IDD microenvironment can be divided into 3 grades, pH 6.2 (severe degeneration), pH 6.4 (moderate degeneration), and pH 6.8 (slight degeneration) [59–62]. With the aggravation of IDD, the acidic stimulation of the residual NPCs and the transplanted stem cells is intensified, further increasing the esterase activation of these cells [9]. Ibuprofen is commonly used for anti-inflammatory treatment and may be applied to inhibit pyroptosis. However, the direct injection of Ibuprofen is rapidly degradable *in vivo*. Accordingly, designing a long-term sustained ibuprofen release system that conforms with the IDD conditions is necessary. Our previous research presented an esterase-responsive nano-micelle delivering system with highly efficient tissue regeneration [9,63]. Therefore, we harnessed an esterase-responsive copolymer ibuprofen nano-micelle PEG-PIB to pre-modify the NPPCs and improve their performance after transplantation.

To build the esterase-responsive ibuprofen sustained-release system, an ibuprofen-based amphiphilic block copolymer nano-micelles was prepared to protect the hydrophobic prodrug core and provide pre-protection for the transplanted stem cells. Specifically, the esterase-responsive ibuprofen copolymer PEG-PIB was prepared to form the nanoparticle. First, Ibuprofen was linked to the 2-hydroxyethyl methacrylate (HEMA), and the monomer obtained was polymerized into a block copolymer through a Reversible Addition-Fragmentation Chain Transfer Polymerization (RAFT) (Fig. 3A). The monomer and the copolymer were characterized by <sup>1</sup>H nuclear magnetic resonance (<sup>1</sup>H NMR) (Fig. 3C and D), which showed that the molecular weight was about 8.5 kDa. Similar results were obtained by the gel permeation chromatography (GPC) (Fig. 3E), with a polydispersity index (PDI) of 1.18. The above results verified that the polymer was successfully obtained. After that, the micelle was prepared through dialysis. The micelle was observed under the scanning electron microscope (Fig. 3B); its size was determined by dynamic light scattering (DLS), which showed a volume-average hydrodynamic diameter of 39.9 nm with a PDI of 0.153 (Fig. 3F). The  $\zeta$  potential of the micelle (Fig. 3G) was  $-6.44 \pm 0.55$  mV when dissolved in pH 7.4 solution showing no significant difference with pH 6.8 solution ( $-7.76 \pm 1.24$  mV), pH 6.4 solution ( $-6.60 \pm 0.21$ ) and pH 6.2 solution ( $-5.02 \pm 0.75$ ). These results indicated the stability and uniformity of the PEG-PIB micelle in different physiological microenvironments. We further assessed the esterase-responsive release of the PEG-PIB micelle. Ibuprofen was gradually released in the presence of 120U/mL porcine esterase, while Ibuprofen was seldomly released from the PEG-PIB without the porcine esterase (Fig. 3H). However, different pH solutions yielded no difference in the release of the Ibuprofen, substantiating that the pH does not affect the micelle.

To further examine the cytocompatibility of PEG-PIB with hNPPCs, we packaged rhodamine into the PEG-PIB and used FACS to prove endocytosis (Fig. 3I). The PEG-PIB was added and co-cultured with hNPPCs; the CCK-8 assay showed no significant effect on the proliferation of hNPPCs. In the meantime, the immunofluorescence results indicated that after 20 min of incubation, PEG-PIB showed higher release efficiency within the hNPPCs in an extracellular microenvironment of pH 6.2 (Fig. 3J). The long-term incubation showed that the sustained release of Ibuprofen within hNPPCs was more efficient in a microenvironment with pH 6.2 (Figure 3M). The acidic stimulation of the transplanted hNPPCs increased the esterase activation and accelerated the release of Ibuprofen from PEG-PIB, which accounted for the high efficiency of the transplanted PEG-PIB pre-modified hNPPCs.

### 3.3. Mechanism of PEG-PIB in inhibiting hNPPCs pyroptosis

Despite the well-preserved functions of NPPCs *in vitro*, pyroptosis remains one of the main causes of death for transplanted stem cells, which has been largely understudied. In IVD samples that underwent the Crenel Lumbar Interbody Fusion (CLIF) operation, we found that the pyroptosis associated proteins and genes were highly expressed in the residual NPCs (Figs. 4A, 4B, 4C & S8B). We further simulated the acidic IDD microenvironment *in vitro* and observed the high expression of ASC within hNPPCs (Fig. 4D and G).

The viability of PEG-PIB pre-modified hNPPCs showed no significant difference at NPEM pHs of 7.4, 6.4 and 6.2, while slightly increased mortality was observed at a pH of 6.8 (Fig. 4E and H), consistent with the CCK-8 results. Meanwhile, the pyroptosis-related ASC expression in PEG-PIB pre-modified hNPPCs decreased with increased acidity (Fig. 4F and I) since increased IDD microenvironment acidity would result in esterase activation in hNPPCs. The PEG-PIB within the pre-modified hNPPCs showed higher efficiency in releasing Ibuprofen at pH 6.2, which further inhibited pyroptosis of transplanted hNPPCs in severe IDD microenvironments.

To better understand the mechanism underlying the inhibitory effect of PEG-PIB on hNPPCs pyroptosis, WB was used to analyze the possible pathways of PEG-PIB. The WB results indicated the significantly reduced protein expression of inflammation-related COX2, p-Ik $\beta$  and IL-1 $\beta$  (Fig. 4K and L) when treated with Ibuprofen and PEG-PIB, while PEG-PETTC showed no significant effect with hNPPCs. In the meantime, pyroptosis-specific protein expressions were examined; NLRP3, ASC and Caspase-1 showed a significant decrease when treated with PEG-PIB. The pre-modification of hNPPCs with PEG-PIB was efficient, which indicated that PEG-PIB played an important role in inhibiting hNPPCs pyroptosis through the COX2/NF- $\kappa$ B/Caspase-1 signaling pathway.

The *in vitro* experimental results indicated that PEG-PIB could significantly decrease both inflammation and pyroptosis in hNPPCs, which provided a promising strategy for inhibiting transplanted hNPPCs pyroptosis. However, the short-term release of Ibuprofen still restricted further application for IDD treatment. Indeed, the injection of PEG-PIB could only temporarily protect the transplanted hNPPCs to pass the acute stage of IDD, emphasizing the need to design long-term sustained-release micelles requires further research to cover the whole therapeutic process of IDD. Altogether, through the endocytosis of PEG-PIB, the hNPPCs were pre-modified to prevent pyroptosis under harsh IDD microenvironments, enabling the hNPPCs to play a better role in IDD regeneration *in vivo*.

### 3.4. Radiographic, MRI and elasticity modulus assessment of IVDs

We further examined the functional regeneration capacity of PEG-PIB pre-modified hNPPCs *in vivo*. 80 male SD rats were divided into five groups (detailed grouping provided in section 2.16 animal procedure).

Fig. 5A shows the disc height results of different groups at each time point. The disc height index% (DHI%) was measured using the formula provided in Fig. 5B. The DHI% of the NC group was associated with a significantly higher index than the DC, PB, and NPPC groups at all four time points. At 6, 10 and 18 weeks, the PB-NPPC group yielded a better regeneration effect than the DC, PB, and NPPC groups. The index of the PB-NPPC group showed no significant difference from the NC group at 18 weeks, indicating the success of PB-NPPC regeneration. The relative DHI% quantitative statistics are provided in Fig. 5C.

Then we observed the structure and water content of IVD tissue using MRI assessment (Fig. 5C). The sagittal and transverse plane results of the disc are shown in Fig. 5D and E, respectively. At all 4 time points, the water content index was significantly higher in the NC group than in any other group. Meanwhile, the PB-NPPC group was higher than DC, PB and NPPC groups at 6, 10 and 18 weeks after modeling. In the transverse plane of the NP tissue, the PB-NPPC group possessed a significantly

higher water content index than DC, PB and NPPC groups after 18 weeks of modeling, while the PB-NPPC group showed no significant difference from the PB and NPPC groups at 10 weeks.

The elasticity modulus force-displacement curve (Figure S5C, S5D & S5E) of the NC group at 6, 10, and 18 weeks were all significantly higher, suggesting it took more loading stress to get to the plateau than in the other four groups; the DC group was the lowest. After 18 weeks, the difference between NPPC and PB-NPPC groups was not significant; the two groups almost coincided on the force-displacement curve.

The radiographic and MRI results indicated that the injection of PEG-PIB modified hNPPCs could significantly improve the disc height and water content of degenerated IVDs. The elasticity modulus of IVDs indicated that the degeneration of IVDs resulted in NP shrinkage and annulus fibrosus (AF) loosening, leading to a decrease in the elasticity modulus. This phenomenon was relieved to a certain extent by both PB and NPPC, which were not as efficient as PEG-PIB pre-modified hNPPCs. These results indicated that the combination strategy of PEG-PIB modified hNPPCs exhibited promising *in vivo* regeneration capacity for improving the physical characteristics of degenerated IVDs.

### 3.5. Histological and immunohistochemical analysis of IVDs

According to the histological grading scale, the IDD pathology degree can be categorized into 3 grades (slight, moderate, and severe degeneration). H&E and S–O staining (Fig. 6A and B) indicated that the NC group presented a mixture of small chondrocyte-like cells and larger vacuolated cells; the annulus fibrosus was well organized with lamellar sheets of collagen. The relative histological grading scores of the DC, PB and NPPC groups were higher than the NC group, with the PB-NPPC group showing a promising therapeutic effect (Fig. 7B). In the DC group, there was significant degeneration of NP after 18 weeks of degeneration; the AF was squeezed into the NP, leaving little or no disordered NP cells. The AF of the PB group was still narrow and exhibited a disordered arrangement after 18 weeks, the injured regions were filled with fibrous connective tissues, but there was still some NP left, which preserved some of the functions of the IVD. Meanwhile, with or without PEG-PIB pre-modified hNPPCs injection, the ECM arrangement and AF structure were compared in the DC and PB groups, but the NP was more plumped and the relative disc height and NP structure in PB-NPPC group appear much better than NPPC group.

The distribution of Collagen II and Aggrecan (Figs. 7A and 8A) in the IVD of the NC group was comparable at 2 and 18 weeks, with positive S–O staining results. At 2 weeks after molding, the IHC results demonstrated that Collagen II and Aggrecan expression in DC, PB, NPPC and PB-NPPC groups was significantly decreased. The NPPC group at 18 weeks showed significant collagen II positive compared with other groups and the PB-NPPC group at 2 weeks. Similar results were also shown with Aggrecan expression. The morphological characteristics of the NPPC group at 18 weeks showed little difference from the PB-NPPC group, while Collagen II and Aggrecan expression was significantly different.

### 3.6. Immunofluorescence analysis of IVDs

The hNPPCs were transfected with GFP lentivirus to trace their function after transplantation. Fewer GFP positive spots were observed in the NPPC group, indicating that transplanted hNPPCs suffered in a harsh IDD microenvironment in the absence of pre-modifying PEG-PIB. The residual hNPPCs struggled to achieve functional regeneration in IDD. The colocalization IF staining showed a high intensity of ASC protein expression in the NPPC group, significantly higher than the PB and PB-NPPC groups. In the meantime, the PB-NPPC group showed substantially lower ASC expression, which indicated the well-preserved function of PEG-PIB pre-modified hNPPCs (Fig. 7E).

Although transplantation of hNPPCs enabled efficient regeneration capacity during IDD treatment, the pyroptosis within the IDD

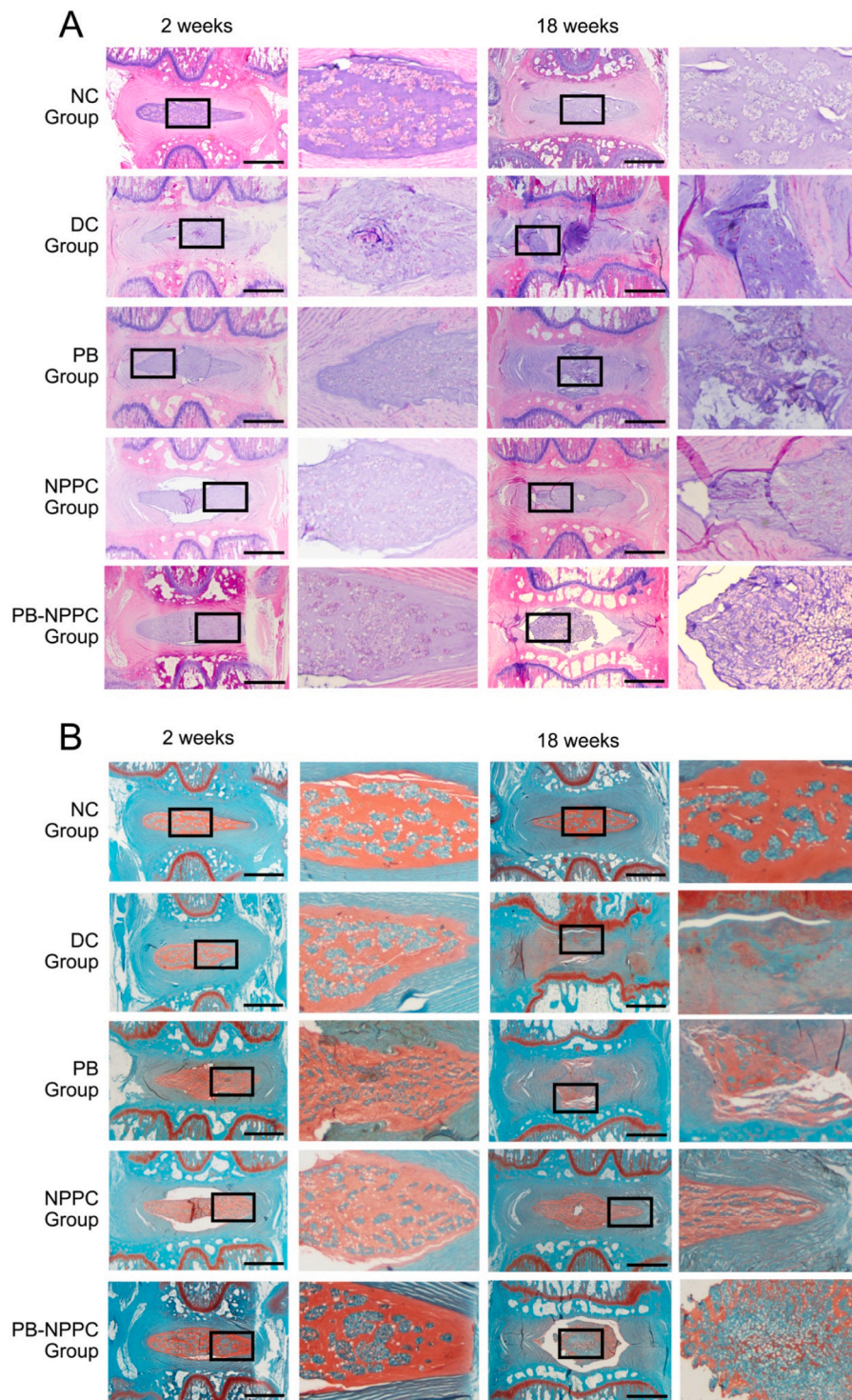


**Fig. 6.** PEG-PIB pre-modified hNPPCs histopathological regeneration results *in vivo*. (A) Representative H&E staining of disc samples from different groups at 2 and 18 weeks after modeling. Scale bar = 1000  $\mu\text{m}$  (B) Representative S-O staining of disc samples from different groups at 2 and 18 weeks after modeling. Scale bar = 1000  $\mu\text{m}$ .

microenvironment remained unresolved. Pyroptosis affected transplanted NPPCs and residual NPCs, which would further aggravate the pathophysiology of IDD. Therefore, the PEG-PIB pre-modified hNPPCs transplantation strategy not only enhanced the viability of transplanted hNPPCs but also improved the microenvironment of IDD.

However, several limitations and shortcomings were present in this study. Our rat IDD model underwent experimentation at a relatively early stage (2 weeks after modeling), which is still within the acute

phase of the IDD pathological process and not comparable with human IDD. It should also be borne in mind that the existence of notochord cells in rats' IVDs could influence regeneration. These findings emphasize the need for improved animal models to better simulate the clinical circumstances.

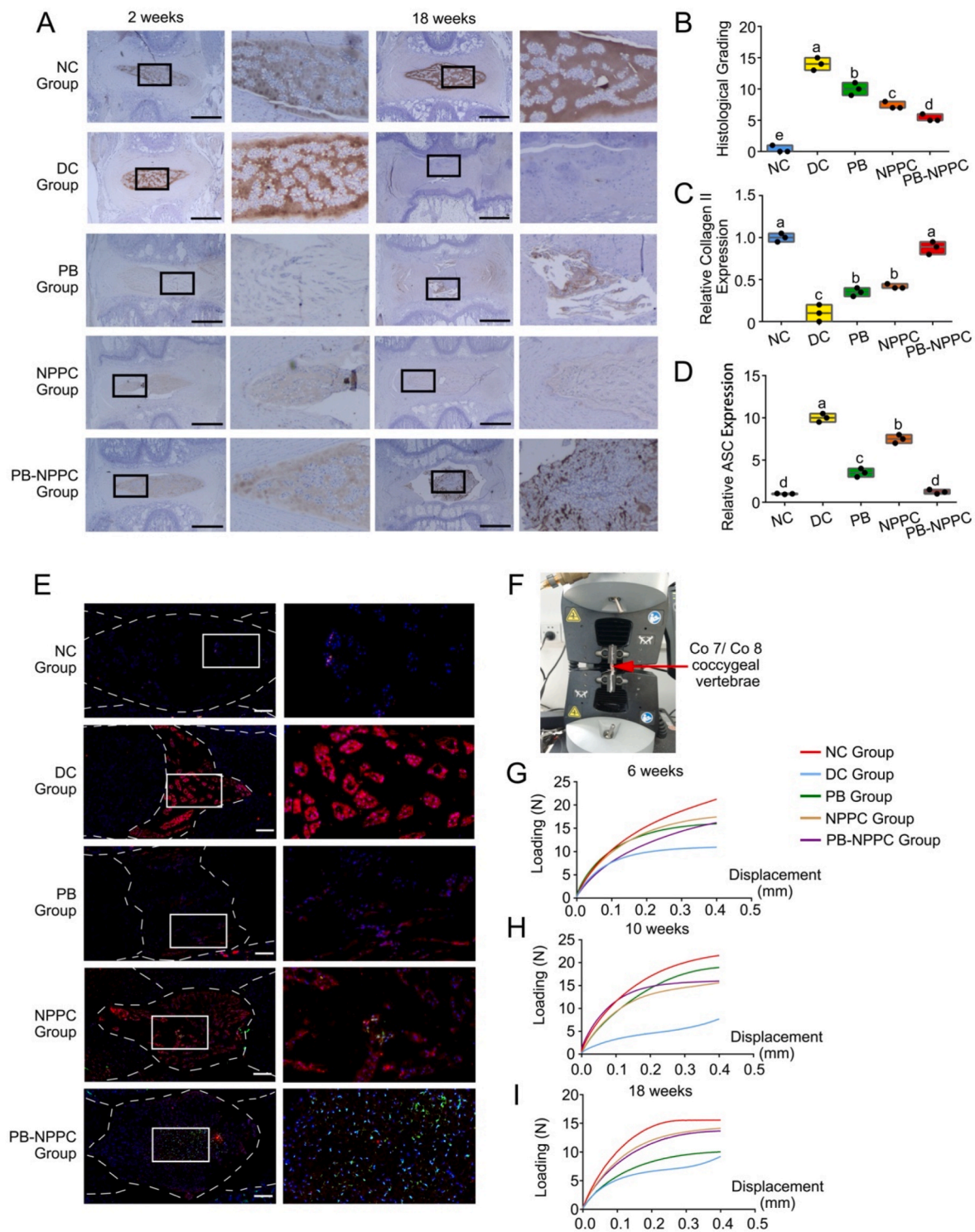


**Fig. 7.** PEG-PIB pre-modified hNPPCs histopathological and functional regeneration results *in vivo*. (A) Immunohistochemistry staining of Collagen II in disc samples from different experimental groups. Scale bar = 1,000  $\mu\text{m}$  (B) Histological scores of all five groups at 18 weeks after modeling.  $p < 0.05$  (one-way ANOVA test) (C) The relative Collagen II expression quantitative analysis of Fig. 7A  $p < 0.05$  (one-way ANOVA test) (D) The relative ASC expression quantitative analysis of Fig. 7E. (one-way ANOVA test) (E) hNPPC tracer (Green) and ASC (Red) immunofluorescence co-location results at 18 weeks after modeling. Dotted lines are the region of NP. (F) The scheme of elasticity modulus. The red arrow points at the coccygeal vertebrae Co 7/Co 8. (G, H and I) The force-displacement curve of all five groups at 6, 10 and 18 weeks after modeling.

#### 4. Conclusion

In this study, our Ibuprofen esterase-responsive copolymer nanomicelle pre-modified embryo-derived long-term expandable NPPCs provide a novel synergistic transplantation strategy. It integrates the

advantages of both cell- and nanoparticle-based transplantation therapy to confer a superior therapeutic effect. The expandable embryo derived NPPCs established yielded higher proliferative ability, stronger nucleus pulposus differentiative capacity and superior IDD microenvironment adaptability than MSCs and PSCs. The esterase-responsive Ibuprofen

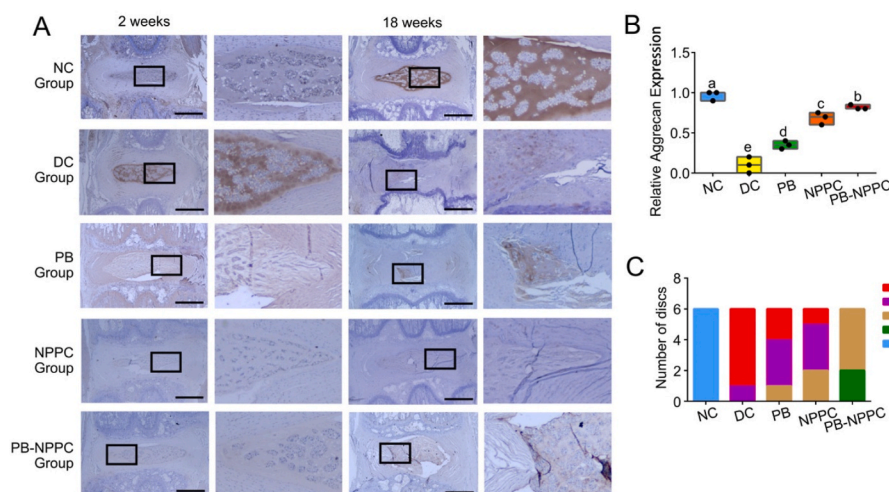


**Fig. 8.** PEG-PIB pre-modified hNPCs histopathological and Pfirrmann grading (A) Immunohistochemistry staining of Aggrecan in disc samples from different experimental groups. Scale bar = 1,000  $\mu$ m (B) The relative Aggrecan I expression quantitative analysis of Fig. 8A  $p < 0.05$  (one-way ANOVA test) (C) The Pfirrmann grading system of different experimental groups were used to quantify the structure, distinction of nucleus and annulus fibrosus, signal intensity, and height of intervertebral disc at 18 weeks. Sample numbers  $N = 6$ .

nano-micelle PEG-PIB further enhanced the adaptability of NPPCs to a harsh IDD microenvironment and enhanced their performance in IDD repairment. In conclusion, research on NPPCs is still in its preliminary stages, with many areas to be explored before clinical translation, such as the alternative for the Matrigel, the exploration of hiPSC-hNPPCs and the long-term preservation of NPPCs' characteristics. Our biomaterial pre-modification strategy of PEG-PIB pre-modified NPPCs offers a promising synergistic transplantation approach for IDD regeneration.

#### Author contributions

Kai-shun Xia, Dong-dong Li and Cheng-gui Wang contribute equally to this work. Kaishun Xia, Qi-xin Chen and Cheng-zhen Liang designed experiments; Kai-shun Xia, Cheng-gui Wang, Li-wei Ying, Jing-kai Wang, Biao Yang, Jia-wei Shu, Xian-peng Huang, Yu-ang Zhang and Chao Yu carried out experiments; Kai-shun Xia, Xiao-peng Zhou and Dong-dong Li analyzed experimental results; Kai-shun Xia wrote the manuscript; Fang-cai Li, Xiao-peng Zhou, Nigel K. H. Slater and Jian-bin Tang helped to polish this manuscript. And all authors critically read and revised the manuscript and approved its submission for publication.

#### Declaration of competing interest

All authors declare that they have no conflict of interest.

#### Acknowledgments

This study was supported by grants from the Nature Science Foundation of Zhejiang Province (Y20H060063, LY19H060005, LQ18H060003, LZ22H090003), the National Natural Science Foundation of China (NO.82072465, NO.81772379, NO.81972096, NO.82172457, NO.82002327), the China Postdoctoral Science Foundation (2017M612011) and the Scientific Research Fund of Zhejiang Provincial Education Department (Y201941476).

#### Abbreviation

IDD	intervertebral disc degeneration
IVD	intervertebral disc
NP	nucleus pulposus
NPCs	nucleus pulposus cells
NPPCs	nucleus pulposus progenitor cells
PEG-PIB	ibuprofen nano-micelles (PEG-PIB)
ASC	Apoptosis associated speck like protein containing a CARD
MSC	mesenchymal stem cells

PSC	pluripotent stem cells
Tie 2	tyrosine kinase receptor 2
GA	gestation age
FACS	flow cytometry
NPEM	NPPC expansion medium
bFGF	basic Fibroblast Growth Factor
BSA	bovine serum albumin
WB	Western Blot
ITS	Insulin-Transferrin-Selenium
TGF- $\beta$ 1	Transforming Growth Factor- $\beta$ 1
GDF-5	Growth Differentiation Factor 5
BMP-2	Bone Morphogenetic Protein
KRT 19	Keratin 19
ESCs	embryonic stem cells
iPSCs	induced pluripotent stem cells
NC group:	The normal control group, without needle puncture or DMEM injection
DC group:	the degeneration control group, needle puncture after 2 weeks and then injected with DMEM injection
PB group:	needle puncture after 2 weeks and then injected with PEG-PIB
NPPC group:	needle puncture after 2 weeks and then injected with hNPPCs
PB-NPPC group:	needle puncture after 2 weeks and then injected with PEG-PIB modified hNPPCs

#### Appendix A. Supplementary data

Supplementary data to this article can be found online at <https://doi.org/10.1016/j.bioactmat.2022.07.024>.

#### References

- [1] M. Zhou, H. Wang, X. Zeng, P. Yin, J. Zhu, W. Chen, X. Li, L. Wang, L. Wang, Y. Liu, J. Liu, M. Zhang, J. Qi, S. Yu, A. Afshin, E. Gakidou, S. Glenn, V.S. Krish, M. K. Miller-Petrie, W.C. Mountjoy-Venning, E.C. Mullany, S.B. Redford, H. Liu, M. Naghavi, S.I. Hay, L. Wang, C.J.L. Murray, X. Liang, Mortality, morbidity, and risk factors in China and its provinces, 1990-2017: a systematic analysis for the Global Burden of Disease Study 2017, *Lancet* 394 (10204) (2019) 1145–1158.
- [2] J.L. Dieleman, J. Cao, A. Chapin, C. Chen, Z. Li, A. Liu, C. Horst, A. Kaldjian, T. Matyas, K.W. Scott, A.L. Bui, M. Campbell, H.C. Duber, A.C. Dunn, A. D. Flaxman, C. Fitzmaurice, M. Naghavi, N. Sadat, P. Shieh, E. Squires, K. Yeung, C. J.L. Murray, US health Care spending by payer and health condition, *JAMA* 323 (9) (2020) 863–884, 1996-2016.
- [3] C.L. Le Maitre, A.J. Freemont, J.A. Hoyland, Accelerated cellular senescence in degenerate intervertebral discs: a possible role in the pathogenesis of intervertebral disc degeneration, *Arthritis Res. Ther.* 9 (3) (2007) R45.
- [4] H.E. Gruber, J.A. Ingram, H.J. Norton, E.N. Hanley Jr., Senescence in cells of the aging and degenerating intervertebral disc: immunolocalization of senescence-

- associated beta-galactosidase in human and sand rat discs, *Spine (Phila Pa 1976 32)* 3 (2007) 321–327.
- [5] F.C. Bach, D.W. Poramba-Liyanaage, F.M. Riemers, J. Guicheux, A. Camus, J. C. Iatridis, D. Chan, K. Ito, C.L. Le Maitre, M.A. Tryfonidou, Notochordal cell-based treatment strategies and their potential in intervertebral disc regeneration, *Front. Cell Dev. Biol.* 9 (2021), 780749.
- [6] A.H. Barakat, V.A. Elwell, K.S. Lam, Stem cell therapy in discogenic back pain, *J. Spine Surg.* 5 (4) (2019) 561–583.
- [7] B.D. Harfe, Intervertebral disc repair and regeneration: insights from the notochord, *Semin. Cell Dev. Biol.* 127 (2022) 3–9.
- [8] I. Martin, J. Galipeau, C. Kessler, K. Le Blanc, F. Dazzi, Challenges for mesenchymal stromal cell therapies, *Sci. Transl. Med.* 11 (480) (2019).
- [9] C. Yu, D. Li, C. Wang, K. Xia, J. Wang, X. Zhou, L. Ying, J. Shu, X. Huang, H. Xu, B. Han, Q. Chen, F. Li, J. Tang, C. Liang, N. Slater, Injectable kartogenin and apocynin loaded micelle enhances the alleviation of intervertebral disc degeneration by adipose-derived stem cell, *Bioact. Mater.* 6 (10) (2021) 3568–3579.
- [10] Y. Zeng, C. Chen, W. Liu, Q. Fu, Z. Han, Y. Li, S. Feng, X. Li, C. Qi, J. Wu, D. Wang, C. Corbett, B.P. Chan, D. Ruan, Y. Du, Injectable microcryogels reinforced alginate encapsulation of mesenchymal stromal cells for leak-proof delivery and alleviation of canine disc degeneration, *Biomaterials* 59 (2015) 53–65.
- [11] G. Feng, Z. Zhang, M. Dang, K.J. Rambahia, P.X. Ma, Nanofibrous spongy microspheres to deliver rabbit mesenchymal stem cells and anti-miR-199a to regenerate nucleus pulposus and prevent calcification, *Biomaterials* 256 (2020), 120213.
- [12] J. Zhu, K. Xia, W. Yu, Y. Wang, J. Hua, B. Liu, Z. Gong, J. Wang, A. Xu, Z. You, Q. Chen, F. Li, H. Tao, C. Liang, Sustained release of GDF5 from a designed coacervate attenuates disc degeneration in a rat model, *Acta Biomater.* 86 (2019) 300–311.
- [13] X. Zhou, J. Wang, W. Fang, Y. Tao, T. Zhao, K. Xia, C. Liang, J. Hua, F. Li, Q. Chen, Genipin cross-linked type II collagen/chondroitin sulfate composite hydrogel-like cell delivery system induces differentiation of adipose-derived stem cells and regenerates degenerated nucleus pulposus, *Acta Biomater.* 71 (2018) 496–509.
- [14] Y. Zhang, Z. Zhang, P. Chen, C.Y. Ma, C. Li, T.Y.K. Au, V. Tam, Y. Peng, R. Wu, K.M. C. Cheung, P.C. Sham, H.F. Tse, D. Chan, V.Y. Leung, K.S.E. Cheah, Q. Lian, Directed differentiation of notochord-like and nucleus pulposus-like cells using human pluripotent stem cells, *Cell Rep.* 30 (8) (2020) 2791–2806, e5.
- [15] R. Tang, L. Jing, V.P. Willard, C.L. Wu, F. Guilak, J. Chen, L.A. Setton, Differentiation of human induced pluripotent stem cells into nucleus pulposus-like cells, *Stem Cell Res. Ther.* 9 (1) (2018) 61.
- [16] D. Sheyn, S. Ben-David, W. Tawackoli, Z. Zhou, K. Salehi, M. Bez, S. De Mel, V. Chan, J. Roth, P. Avalos, J.C. Giaconii, H. Yameen, L. Hazanov, D. Seliktar, D. Li, D. Gazit, Z. Gazit, Human iPSCs can be differentiated into notochordal cells that reduce intervertebral disc degeneration in a porcine model, *Theranostics* 9 (25) (2019) 7506–7524.
- [17] Y. Liu, M.N. Rahaman, B.S. Bal, Modulating notochordal differentiation of human induced pluripotent stem cells using natural nucleus pulposus tissue matrix, *PLoS One* 9 (7) (2014), e100885.
- [18] Y. Liu, S. Fu, M.N. Rahaman, J.J. Mao, B.S. Bal, Native nucleus pulposus tissue matrix promotes notochordal differentiation of human induced pluripotent stem cells with potential for treating intervertebral disc degeneration, *J. Biomed. Mater. Res. A* 103 (3) (2015) 1053–1059.
- [19] K. Liu, Z. Chen, X.W. Luo, G.Q. Song, P. Wang, X.D. Li, M. Zhao, X.W. Han, Y. G. Bai, Z.L. Yang, G. Feng, Determination of the potential of induced pluripotent stem cells to differentiate into mouse nucleus pulposus cells in vitro, *Genet. Mol. Res.* 14 (4) (2015) 12394–12405.
- [20] T. Kamatani, H. Hagizawa, S. Yarimitsu, M. Morioka, S. Koyamatsu, M. Sugimoto, J. Kodama, Y. Yamane, H. Ishiguro, S. Shichino, K. Abe, W. Fujibuchi, H. Fujie, T. Kaito, N. Tsumaki, Human iPSC cell-derived cartilaginous tissue spatially and functionally replaces nucleus pulposus, *Biomaterials* 284 (2022), 121491.
- [21] P. Colombier, B. Halgand, C. Chédeville, C. Chariav, V. François-Campion, S. Kilens, N. Vedrenne, J. Clouet, L. David, J. Guicheux, A. Camus, NOTO transcription factor directs human induced pluripotent stem cell-derived mesoderm progenitors to a notochordal fate, *Cells* 9 (2) (2020).
- [22] J. Chen, E.J. Lee, L. Jing, N. Christoforou, K.W. Leong, L.A. Setton, Differentiation of mouse induced pluripotent stem cells (iPSCs) into nucleus pulposus-like cells in vitro, *PLoS One* 8 (9) (2013), e75548.
- [23] K. Xia, J. Zhu, J. Hua, Z. Gong, C. Yu, X. Zhou, J. Wang, X. Huang, W. Yu, L. Li, J. Gao, Q. Chen, F. Li, C. Liang, Intradiscal injection of induced pluripotent stem cell-derived nucleus pulposus-like cell-seeded polymeric microspheres promotes rat disc regeneration, *Stem Cell Int.* 2019 (2019), 6806540.
- [24] J.F. Blanco, I.F. Graciani, F.M. Sanchez-Guijo, S. Muntión, P. Hernandez-Campo, C. Santamaria, S. Carrancio, M.V. Barbado, G. Cruz, S. Gutierrez-Cosío, C. Herrero, J.F. San Miguel, J.G. Brinon, M.C. del Cañizo, Isolation and characterization of mesenchymal stromal cells from human degenerated nucleus pulposus: comparison with bone marrow mesenchymal stromal cells from the same subjects, *Spine (Phila Pa 1976 35)* 26 (2010) 2259–2265.
- [25] W.M. Erwin, D. Islam, R.D. Inman, M.G. Fehlings, F.W. Tsui, Notochordal cells protect nucleus pulposus cells from degradation and apoptosis: implications for the mechanisms of intervertebral disc degeneration, *Arthritis Res. Ther.* 13 (6) (2011) R215.
- [26] L.T. Liu, B. Huang, C.Q. Li, Y. Zhuang, J. Wang, Y. Zhou, Characteristics of stem cells derived from the degenerated human intervertebral disc cartilage endplate, *PLoS One* 6 (10) (2011), e26285.
- [27] M.V. Risbud, A. Guttapalli, T.T. Tsai, J.Y. Lee, K.G. Danielson, A.R. Vaccaro, T. J. Albert, Z. Gazit, D. Gazit, I.M. Shapiro, Evidence for skeletal progenitor cells in the degenerate human intervertebral disc, *Spine (Phila Pa 1976 32)* (2007) 2537–2544.
- [28] D. Sakai, Y. Nakamura, T. Nakai, T. Mishima, S. Kato, S. Grad, M. Alini, M. V. Risbud, D. Chan, K.S. Cheah, K. Yamamura, K. Masuda, H. Okano, K. Ando, J. Mochida, Exhaustion of nucleus pulposus progenitor cells with ageing and degeneration of the intervertebral disc, *Nat. Commun.* 3 (2012) 1264.
- [29] B. Gao, B. Jiang, W. Xing, Z. Xie, Z. Luo, W. Zou, Discovery and application of postnatal nucleus pulposus progenitors essential for intervertebral disc homeostasis and degeneration, *Adv Sci (Weinh)* 9 (13) (2022), e2104888.
- [30] F.J. Lyu, K.M. Cheung, Z. Zheng, H. Wang, D. Sakai, V.Y. Leung, IVD progenitor cells: a new horizon for understanding disc homeostasis and repair, *Nat. Rev. Rheumatol.* 15 (2) (2019) 102–112.
- [31] Z. Liao, H. Liu, L. Ma, J. Lei, B. Tong, G. Li, W. Ke, K. Wang, X. Feng, W. Hua, S. Li, C. Yang, Engineering extracellular vesicles restore the impaired cellular uptake and attenuate intervertebral disc degeneration, *ACS Nano* 15 (9) (2021) 14709–14724.
- [32] N.S. Woodling, D. Colas, Q. Wang, P. Minhas, M. Panchal, X. Liang, S.D. Mhatre, H. Brown, N. Ko, I. Zagol-Ikapitte, M. van der Hart, T.V. Khroyan, B. Chuluun, P. G. Priyam, G.L. Milne, A. Rassoulpour, O. Boutaud, A.B. Manning-Boğ, H.C. Heller, K.I. Andreasson, Cyclooxygenase inhibition targets neurons to prevent early behavioural decline in Alzheimer's disease model mice, *Brain* 139 (Pt 7) (2016) 2063–2081.
- [33] S.R. Alves Rico, A.Z. Abbasi, G. Ribeiro, T. Ahmed, X.Y. Wu, D. de Oliveira Silva, Diruthenium(ii,iii) metallodrugs of ibuprofen and naproxen encapsulated in intravenously injectable polymer-lipid nanoparticles exhibit enhanced activity against breast and prostate cancer cells, *Nanoscale* 9 (30) (2017) 10701–10714.
- [34] D. Sakai, J. Schol, F.C. Bach, A. Tekari, N. Sagawa, Y. Nakamura, S.C.W. Chan, T. Nakai, L.B. Creemers, D.A. Frauchiger, R.D. May, S. Grad, M. Watanabe, M. A. Tryfonidou, B. Gantenbein, Successful fishing for nucleus pulposus progenitor cells of the intervertebral disc across species, *JOR Spine* 1 (2) (2018), e1018.
- [35] A. Tekari, S.C.W. Chan, D. Sakai, S. Grad, B. Gantenbein, Angiopoietin-1 receptor Tie2 distinguishes multipotent differentiation capability in bovine coccygeal nucleus pulposus cells, *Stem Cell Res. Ther.* 7 (1) (2016) 75.
- [36] K. Sako, D. Sakai, Y. Nakamura, J. Schol, E. Matsushita, T. Warita, N. Horikita, M. Sato, M. Watanabe, Effect of whole tissue culture and basic fibroblast growth factor on maintenance of Tie2 molecule expression in human nucleus pulposus cells, *Int. J. Mol. Sci.* 22 (9) (2021).
- [37] L. Xue, H. Yi, Z. Huang, Y.B. Shi, W.X. Li, Global gene expression during the human organogenesis: from transcription profiles to function predictions, *Int. J. Biol. Sci.* 7 (7) (2011) 1068–1076.
- [38] V. Sivakamasundari, T. Lufkin, Bridging the gap: understanding embryonic intervertebral disc development, *Cell Dev. Biol.* 1 (2) (2012).
- [39] K.S. Choi, B.D. Harfe, Hedgehog signaling is required for formation of the notochord sheath and patterning of nuclei pulposi within the intervertebral discs, *Proc. Natl. Acad. Sci. U. S. A.* 108 (23) (2011) 9484–9489.
- [40] Z. Li, T. Araoka, J. Wu, H.K. Liao, M. Li, M. Lazo, B. Zhou, Y. Sui, M.Z. Wu, I. Tamura, Y. Xia, E. Beyret, T. Matsusaka, I. Pastan, C. Rodriguez Esteban, I. Guillen, P. Guillen, J.M. Campistol, J.C. Izpisua Belmonte, 3D culture supports long-term expansion of mouse and human nephrogenic progenitors, *Cell Stem Cell* 19 (4) (2016) 516–529.
- [41] H. Hu, H. Gehart, B. Artegiani, C. López-Iglesias, F. Dekkers, O. Basak, J. van Es, S. M. Chuva de Sousa Lopes, H. Begthel, J. Korving, M. van den Born, C. Zou, C. Quirk, L. Chiriboga, C.M. Rice, S. Ma, A. Rios, P.J. Peters, Y.P. de Jong, H. Clevers, Long-term expansion of functional mouse and human hepatocytes as 3D organoids, *Cell* 175 (6) (2018) 1591–1606, e19.
- [42] L. Broutier, A. Andersson-Rolf, C.J. Hindley, S.F. Boj, H. Clevers, B.K. Koo, M. Huch, Culture and establishment of self-renewing human and mouse adult liver and pancreas 3D organoids and their genetic manipulation, *Nat. Protoc.* 11 (9) (2016) 1724–1743.
- [43] A. Yamashita, M. Morioka, Y. Yahara, M. Okada, T. Kobayashi, S. Kuriyama, S. Matsuda, N. Tsumaki, Generation of scaffoldless hyaline cartilaginous tissue from human iPSCs, *Stem Cell Rep.* 4 (3) (2015) 404–418.
- [44] M. Semsarilar, E.R. Jones, A. Blanaaz, S.P. Armes, Efficient synthesis of sterically-stabilized nano-objects via RAFT dispersion polymerization of benzyl methacrylate in alcoholic media, *Adv. Mater.* 24 (25) (2012) 3378–3382.
- [45] J.G. de Souza, N. Starobinas, O.C.M. Ibanez, Unknown/enigmatic functions of extracellular ASC, *Immunology* 163 (4) (2021) 377–388.
- [46] A. Lai, J. Gansau, S.E. Gullbrand, J. Crowley, C. Cunha, S. Dudli, J.B. Engiles, M. Fusellier, R.M. Goncalves, D. Nakashima, J. Okewunmi, M. Pelletier, S. M. Presciutti, J. Schol, Y. Takeoka, S. Yang, T. Yurube, Y. Zhang, J.C. Iatridis, Development of a standardized histopathology scoring system for intervertebral disc degeneration in rat models: an initiative of the ORS spine section, *JOR Spine* 4 (2) (2021), e1150.
- [47] R. Rodrigues-Pinto, A. Berry, K. Piper-Hanley, N. Hanley, S.M. Richardson, J. A. Hoyland, Spatiotemporal analysis of putative notochordal cell markers reveals CD24 and keratins 8, 18, and 19 as notochord-specific markers during early human intervertebral disc development, *J. Orthop. Res.* 34 (8) (2016) 1327–1340.
- [48] C.L. Korecki, J.M. Taboas, R.S. Tuan, J.C. Iatridis, Notochordal cell conditioned medium stimulates mesenchymal stem cell differentiation toward a young nucleus pulposus phenotype, *Stem Cell Res. Ther.* 1 (2) (2010) 18.
- [49] S. Illien-Jünger, B. Gantenbein-Ritter, S. Grad, P. Lezuou, S.J. Ferguson, M. Alini, K. Ito, The combined effects of limited nutrition and high-frequency loading on intervertebral discs with endplates, *Spine (Phila Pa 1976 35)* (19) (2010) 1744–1752.
- [50] S. Illien-Jünger, G. Pattappa, M. Peroglio, L.M. Benneker, M.J. Stoddart, D. Sakai, J. Mochida, S. Grad, M. Alini, Homing of mesenchymal stem cells in induced

- degenerative intervertebral discs in a whole organ culture system, *Spine (Phila Pa 1976)* 37 (22) (2012) 1865–1873.
- [51] G. Pattappa, M. Peroglio, D. Sakai, J. Mochida, L.M. Benneker, M. Alini, S. Grad, CCL5/RANTES is a key chemoattractant released by degenerative intervertebral discs in organ culture, *Eur. Cell. Mater.* 27 (2014) 124–136. ; discussion 136.
- [52] H. Henriksson, M. Thornemo, C. Karlsson, O. Hägg, K. Junevik, A. Lindahl, H. Brisby, Identification of cell proliferation zones, progenitor cells and a potential stem cell niche in the intervertebral disc region: a study in four species, *Spine (Phila Pa 1976)* 34 (21) (2009) 2278–2287.
- [53] W.C. Tzaan, H.C. Chen, Investigating the possibility of intervertebral disc regeneration induced by granulocyte colony stimulating factor-stimulated stem cells in rats, *Adv. Orthop.* 2011 (2011), 602089.
- [54] D. Sakai, K. Nishimura, M. Tanaka, D. Nakajima, S. Grad, M. Alini, H. Kawada, K. Ando, J. Mochida, Migration of bone marrow-derived cells for endogenous repair in a new tail-looping disc degeneration model in the mouse: a pilot study, *Spine J.* 15 (6) (2015) 1356–1365.
- [55] S. Kim, S. Min, Y.S. Choi, S.H. Jo, J.H. Jung, K. Han, J. Kim, S. An, Y.W. Ji, Y. G. Kim, S.W. Cho, Tissue extracellular matrix hydrogels as alternatives to Matrigel for culturing gastrointestinal organoids, *Nat. Commun.* 13 (1) (2022) 1692.
- [56] A. Dicks, C.L. Wu, N. Steward, S.S. Adkar, C.A. Gersbach, F. Guilak, Prospective isolation of chondroprogenitors from human iPSCs based on cell surface markers identified using a CRISPR-Cas9-generated reporter, *Stem Cell Res. Ther.* 11 (1) (2020) 66.
- [57] B. Paes, L. Stabeli, P.N.M. Costa, M.D. Orellana, S. Kashima, D.T. Covas, V. Picanço-Castro, Generation of hematopoietic stem/progenitor cells with sickle cell mutation from induced pluripotent stem cell in serum-free system, *Hematol. Transfus. Cell Ther.* 43 (2) (2021) 156–164.
- [58] K. Xia, Z. Gong, J. Zhu, W. Yu, Y. Wang, J. Wang, A. Xu, X. Zhou, H. Tao, F. Li, C. Liang, Differentiation of pluripotent stem cells into nucleus pulposus progenitor cells for intervertebral disc regeneration, *Curr. Stem Cell Res. Ther.* 14 (1) (2019) 57–64.
- [59] H. Li, C. Liang, Y. Tao, X. Zhou, F. Li, G. Chen, Q.X. Chen, Acidic pH conditions mimicking degenerative intervertebral discs impair the survival and biological behavior of human adipose-derived mesenchymal stem cells, *Exp. Biol. Med.* (Maywood) 237 (7) (2012) 845–852.
- [60] H. Li, Y. Tao, C. Liang, B. Han, F. Li, G. Chen, Q. Chen, Influence of hypoxia in the intervertebral disc on the biological behaviors of rat adipose- and nucleus pulposus-derived mesenchymal stem cells, *Cells Tissues Organs* 198 (4) (2013) 266–277.
- [61] C.Z. Liang, H. Li, Y.Q. Tao, X.P. Zhou, Z.R. Yang, F.C. Li, Q.X. Chen, The relationship between low pH in intervertebral discs and low back pain: a systematic review, *Arch. Med. Sci.* 8 (6) (2012) 952–956.
- [62] C. Liang, H. Li, Y. Tao, X. Zhou, F. Li, G. Chen, Q. Chen, Responses of human adipose-derived mesenchymal stem cells to chemical microenvironment of the intervertebral disc, *J. Transl. Med.* 10 (2012) 49.
- [63] J. Wang, D. Li, C. Liang, C. Wang, X. Zhou, L. Ying, Y. Tao, H. Xu, J. Shu, X. Huang, Z. Gong, K. Xia, F. Li, Q. Chen, J. Tang, Y. Shen, Scar tissue-targeting polymer micelle for spinal cord injury treatment, *Small* 16 (8) (2020), e1906415.